# New Insights in Molecular Mechanism under Progression of Liver Fibrosis

March 2014

Kotaro Sakata

# 主　論　文　要　旨

| 報告番号 | ㊙ 乙 第　　号 | 氏 名 | 坂田　幸大郎 |
|---|---|---|---|

主 論 文 題 目 ：

New Insights in Molecular Mechanism under Progression of Liver Fibrosis

（肝線維症進展の新しい分子機構解明）

（内容の要旨）

肝線維症は、コラーゲンをはじめとする細胞外基質の過剰な蓄積により引き起こされ、肝硬変や肝癌へと進展する病態である。C 型肝炎ウイルス（HCV）の感染や血管新生は肝線維症を促進することが知られているが、その分子機構については不明な点が残されている。そこで本研究では、線維化誘導サイトカインである TGF-βに着目し、肝線維症進展の新しい分子機構について解析を行った。

**(1) HCV NS3 プロテアーゼの TGF-βⅠ型受容体結合・活性化を介した肝線維化促進機構**

近年、ウイルスが宿主タンパク質を模倣し、細胞機能をハイジャックする現象が報告されている。本研究では、HCV の非構造タンパク質の一つである NS3 プロテアーゼが TGF-β2 の抗原性ならびに生物活性を有していることの発見に端を発し、NS3 の TGF-β疑似活性が肝線維化を促進しているのではないかという作業仮説を立て、検証を行った。TGF-β応答性ルシフェラーゼ発現細胞において、組換え NS3 タンパク質は TGF-βⅠ型受容体を介して TGF-β疑似活性を発現した。また C 型肝炎患者において高い血中濃度を示す腫瘍壊死因子（TNF-α）が TGF-βⅠ型受容体の発現を亢進することにより、肝細胞における NS3 感受性が誘導された。続いて HCV 感染肝癌細胞株において、ウイルス由来の NS3 が細胞表面において TGF-βⅠ型受容体と相互作用することを示した。さらに、NS3 と TGF-βⅠ型受容体のドッキングシミュレーションを行い、予測結合サイトに対する抗 NS3 抗体を作製し、同抗体が HCV 感染ヒト肝細胞移植キメラマウスにおける肝線維化進展を抑制することを示した。これらの結果より、HCV NS3 プロテアーゼは TGF-βを模倣し、そのⅠ型受容体と結合して下流のシグナルを活性化させ、肝線維症の進展に寄与していることが示唆された。

**(2) 新生血管由来潜在型 TGF-βを介した肝線維化促進機構**

肝疾患の進展過程においては線維化と血管新生が並行して起こる。マウスに VEGF を投与し血管新生を誘発させたところ、内皮細胞の指標である CD31 の発現亢進に加えてコラーゲンを多量に産生する活性型肝星細胞の指標であるα-SMA の発現亢進、コラーゲンを構成する特徴的アミノ酸であるヒドロキシプロリン含量が増加した。活性化していない初代培養肝星細胞（HSCs）に VEGF を処理してもα-SMA は亢進しなかったが、初代培養肝類洞内皮細胞（LSECs）の培養上清を HSCs に処理すると、α-SMA の発現が亢進し、その効果は TGF-β1 中和抗体により抑制された。さらに LSECs の培養上清中には潜在型の TGF-βが多量に含まれており、それらが HSCs の細胞表面において活性化され多量の活性型 TGF-βを生じることを見出した。これらの結果より、新生血管は潜在型 TGF-βを供給することにより、肝線維症促進に寄与していることが示唆された。

# SUMMARY OF Ph.D. DISSERTATION

| School | Student Identification Number | SURNAME, First name |
|---|---|---|
| Science and Technology | 81145230 | SAKATA, Kotaro |

Title

New Insights in Molecular Mechanism under Progression of Liver Fibrosis


Abstract

Liver fibrosis is caused by excessive accumulation of extracellular matrix proteins such as collagen. Advanced liver fibrosis leads to cirrhosis, liver failure, and hepatocellular carcinoma. Hepatitis C virus (HCV) infection and angiogenesis are causes of liver fibrosis, although the underlying mechanisms remain to be elucidated. In this thesis, the author documented the molecular mechanism, by which HCV infection and angiogenesis enhanced liver fibrosis, by focusing on transforming growth factor (TGF)-β, the most fibrogenic cytokine.

**(1) HCV NS3 protease enhances liver fibrosis via binding to and activating TGF-β type I receptor**

Viruses sometimes mimic host proteins and hijack the host cell machinery. In this chapter, starting from the discovery that HCV non-structural protein 3 (NS3) protease possesses the antigenicity and bioactivity of TGF-β2, the author explored the working hypothesis that NS3 protease promoted liver fibrosis via TGF-β mimetic activity. Recombinant NS3 protease showed the antigenicity in TGF-β2 ELISA. It exerted bioactivity of TGF-β2 in $(CAGA)_9$-Luc CCL64 cells as well as in human hepatic cell lines via binding to TGF-β type I receptor (TβRI). Tumor necrosis factor (TNF)-α facilitated this mechanism by stimulating the expression of TβRI thus facilitating interaction with NS3 protease on the surface of HCV-infected cells. An anti-NS3 antibody made against computationally predicted binding sites for TβRI blocked the TGF-β mimetic activities of NS3 in vitro and attenuated liver fibrosis in HCV-infected chimeric mice. These data suggest that HCV NS3 protease mimics TGF-β2 and functions, at least in part, via directly binding to and activating TβRI, thereby enhancing liver fibrosis.

**(2) Neovessel formation enhances liver fibrosis via providing with latent TGF-β to HSCs**

Hepatic fibrosis and angiogenesis occur in parallel during the progression of liver diseases. In addition to increased hepatic levels of CD31, a marker of endothelial cells, vascular endothelial growth factor (VEGF)-treated mice showed increased hepatic levels of α-smooth muscle actin (α-SMA), a marker of activated hepatic stellate cells (HSCs), and hepatic hydroxyproline contents. Although cultured HSCs did not show an increase in α-SMA expression when incubated with VEGF, then expressed increased levels of α-SMA when incubated with conditioned medium (CM) from liver sinusoidal endothelial cells (LSECs), which was blocked by the inclusion of neutralizing anti-TGF-β1 antibodies. Indeed, LSEC CM included a huge amount of latent TGF-β, which was activated on the surface of HSCs. These data suggest that angiogenesis may accelerate liver fibrosis via providing with latent TGF-β from increased number of LSECs.

A Thesis for the Degree of Ph.D. in Science

# New Insights in Molecular Mechanism under Progression of Liver Fibrosis

March 2014

Graduate School of Science and Technology

Keio University

Kotaro Sakata

**Contents**

**Abbreviations**

| | |
|---|---|
| α-SMA | alpha-smooth muscle actin |
| CM | conditioned medium |
| ECM | extracellular matrix |
| GPI | glycosylphosphatidylinositol |
| HCC | hepatocellular carcinoma |
| HCV | hepatitis C virus |
| HSC | hepatic stellate cell |
| LAP | latency associated protein |
| LSEC | liver sinusoidal endothelial cells |
| NS3 | non-structural protein 3 |
| PI-PLC | phosphatidylinositol-specific phospholipase C |
| PLA | proximity ligation assay |
| PLK | plasma kallikrein |
| TβRI | TGF-β type I receptor |
| TβRII | TGF-β type II receptor |
| TGF-β | transforming growth factor-beta |
| TNF-α | tumor necrosis factor-alpha |
| uPAR | urokinase-type plasminogen activator receptor |
| VEGF | vascular endothelial growth factor |

# Chapter 1

# General introduction

## 1-1. Liver fibrosis

Liver fibrosis, the wound healing response to chronic liver injury resulting from a variety of stimuli including viral infection, alcohol abuse, and metabolic diseases, is characterized by the excessive accumulation of extracellular matrix (ECM) proteins, including collagen (Fig. 1-1) [1, 2]. Advanced liver fibrosis leads to cirrhosis, portal hypertension, and ultimately to liver failure, eventually causing hepatocellular carcinoma (HCC). Hepatic stellate cells (HSCs) play a pivotal role in the pathogenesis of liver fibrosis by virtue of their ability to undergo a process termed activation [2, 3]. Under physiological conditions, quiescent HSCs embrace sinusoids as liver-specific pericytes. When the liver parenchyma is chronically injured by various causes, HSCs detach from the sinusoids and subsequently transform into myofibroblast-like cells (HSC activation), which is characterized by a loss of lipid droplets, the enhanced production of ECM, and the expression of α-smooth muscle actin (α-SMA) and other activation markers [3]. A process of HSC activation is regulated by both autocrine and paracrine growth factors [3, 4]. One of the key factors promoting HSC activation is transforming growth factor (TGF)-β, the most fibrogenic cytokine, which plays a critical role in the pathogenesis of liver diseases [5, 6].

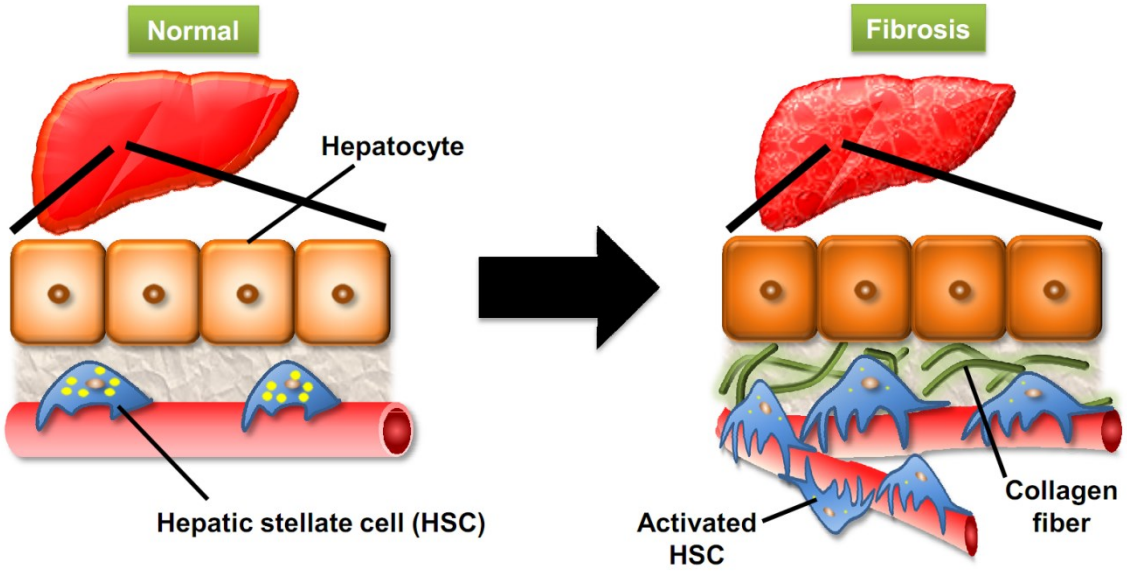


**Figure 1-1. The pathogenesis of liver fibrosis**

## 1-2. TGF-β

TGF-β is produced as a high molecular weight latent form with a dimer consisting of a 75 kD propeptide region called as latency associated protein (LAP), which remains associate with a 25 kD active TGF-β by non-covalent bonds [7, 8]. This complex is S-S bonded to the latent TGF-β binding protein, a component of the ECM, and active TGF-β exerts its biological activity when it is released from its complex through the proteolytic cleavage of LAP, by serine proteases, such as plasmin and plasma kallikrein (PLK), associated with glycosylphosphatidylinositol (GPI)-anchored urokinase-type plasminogen activator receptor (uPAR) on the cell surface (Fig. 1-2) [9].

The resultant active TGF-β binds to TGF-β type II receptor (TβRII) and then recruits type I receptor (TβRI) to form a heterotetrameric active receptor complex that results in the phosphorylation of TβRI by TβRII, inducing the phosphorylation of Smad2/3, which then binds to Smad4 and forms a complex that enters the cell nucleus. This complex acts as a transcription factor that controls the expression of target genes, including collagen and TGF-β itself, by binding to the DNA elements containing the minimal Smad-binding element, CAGA box ,which is located in promoter region of the target genes [10].

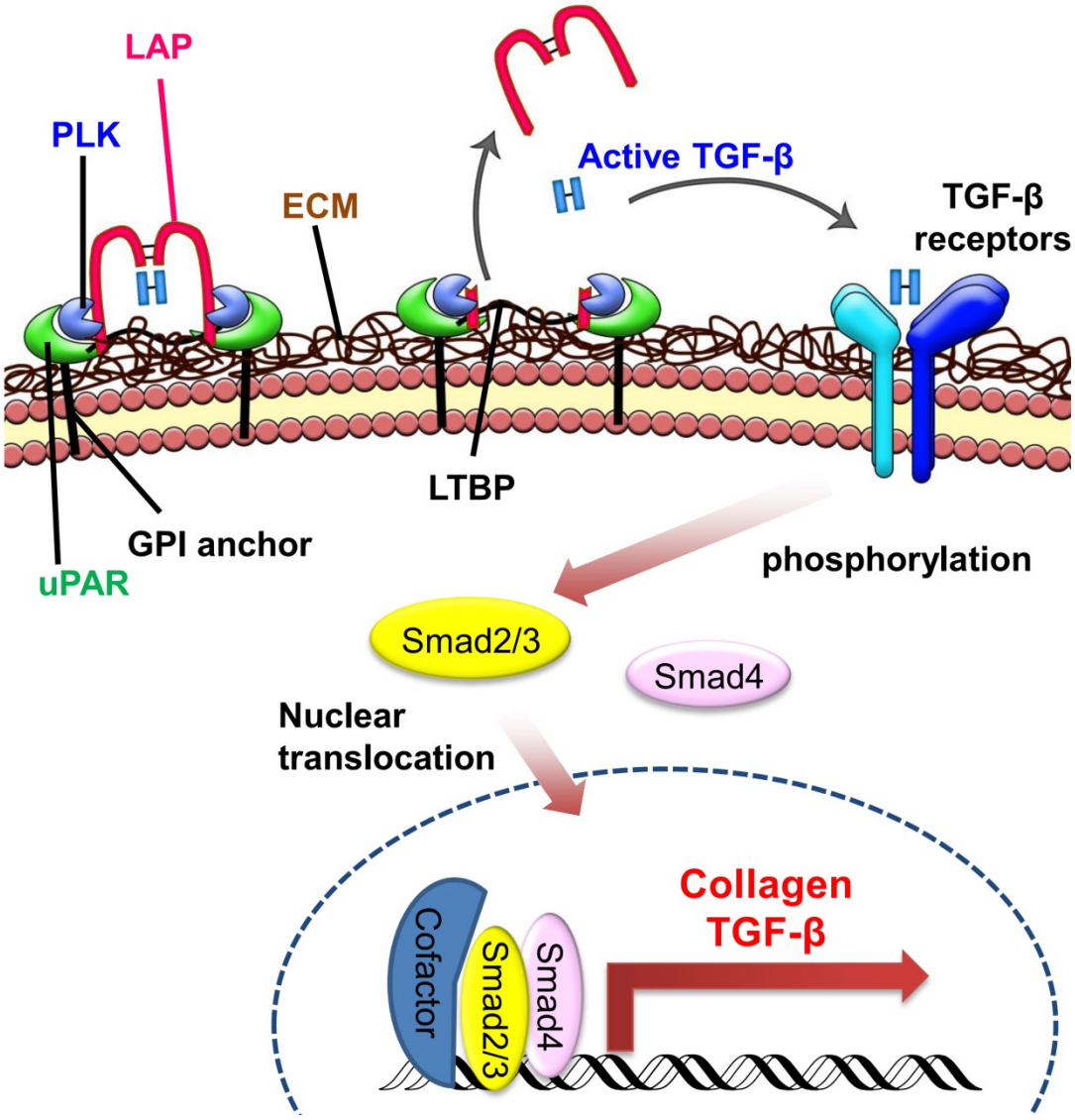


**Figure 1-2. TGF-β activation and its signaling pathway**

## 1-3. Hepatitis C virus (HCV)

An estimated 130-170 million people worldwide are infected with HCV [11]. HCV, classified in the genus *Hepacivirus* of the family *Flaviviridae*, is a positive-strand RNA virus with an approximately 9.6-kb viral genome encoding structural proteins (core, E1, and E2) forming the viral particle, and non-structural proteins (p7, NS2, NS3, NS4A, NS4B, NS5A, and NS5B) facilitating viral replication and production (Fig. 1-3) [12].

HCV infects humans and chimpanzees, and mainly target their hepatocytes [13]. CD81, a low density lipoprotein receptor, scavenger receptor class B, and claudin-1 have been proposed to work as HCV-binding receptors on host cell surface [14]. After entry into the cell and uncoating, HCV genome is translated to produce a single polyprotein, which is processed by two cellular proteases, signal peptidase and signal peptide peptidase, and two viral proteases, NS2-3 autoprotease and NS3 serine protease associated with its cofactor NS4A, for generating mature viral proteins. Viral RNA synthesized by NS5B RNA-dependent RNA polymerase interacts with core proteins, E1,and E2, which form the virion capsid, followed by the release in concert with production of very low density lipoprotein (Fig. 1-4) [12].

Chronic HCV infection is one of the major causes of liver fibrosis, cirrhosis, and hepatocellular carcinoma [15, 16]. However, the molecular mechanism by which HCV

induces liver fibrosis is not fully understood. To address the mechanism is expected to give a clue to establish new strategy for an anti-fibrotic therapy.

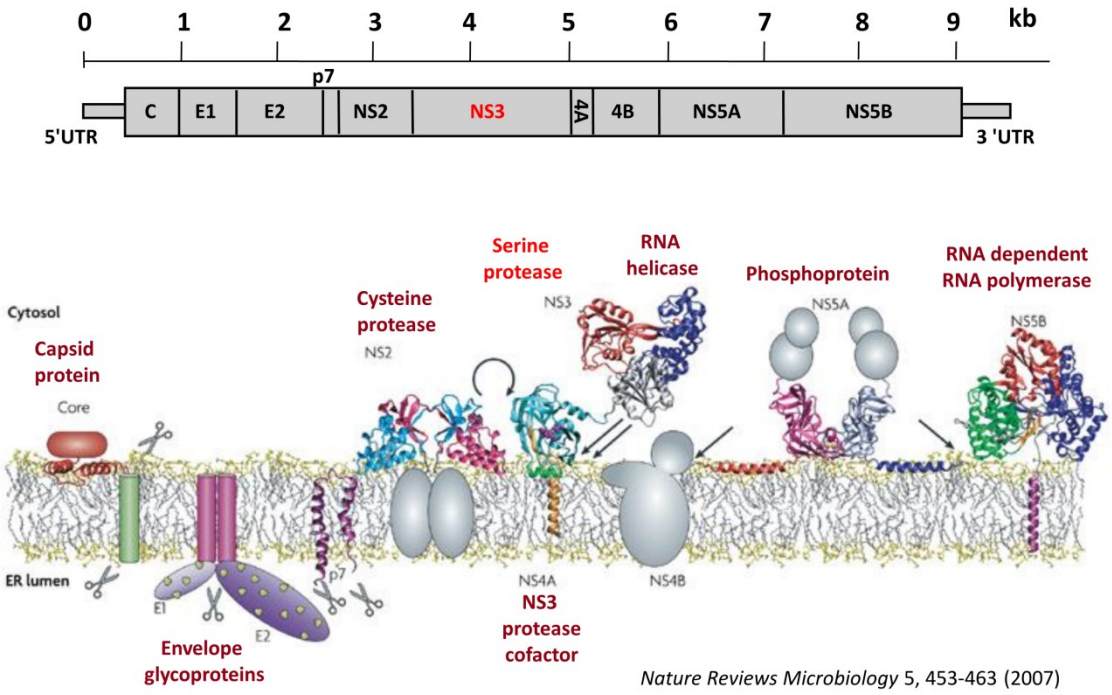


**Figure 1-3. HCV genome and proteins**

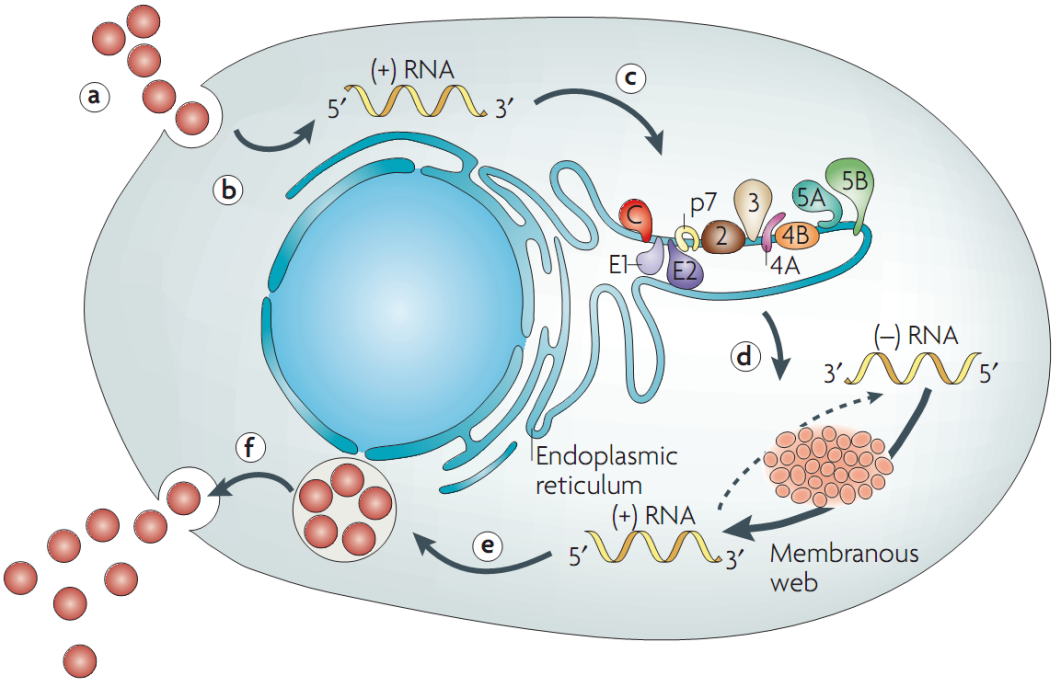


*Nature Reviews Microbiology* 5, 453-463 (2007)

**Figure 1-4. Lifecycle of HCV**

**(a); viral entry (b); translation and polyprotein processing (c); RNA replication (d); viral assembly (e); virion maturation (f); viral release from host cells**

## 1-4. Angiogenesis and fibrosis

Angiogenesis is a dynamic process leading to the formation of new blood vessels from pre-existing blood vessels then lumen formation and eventually stabilization of nascent vessels [17]. In the liver, angiogenesis occurs in pathological settings like cirrhosis and tumor angiogenesis as well as in physiological conditions like liver development and regeneration [18, 19]. Blood vessels in the liver are classified into hepatic artery, portal vein, and sinusoidal blood vessels. Among them, liver sinusoidal endothelial cells (LSECs) are the largest population of endothelial cells in the liver [19].

Vascular endothelial growth factor (VEGF), the most important angiogenic factor, is an approximately 34 to 46 kD homodimeric glycoprotein [20]. It has eight polypeptide-encoding exons and includes several spliced forms with 121, 145, 165, 189, and 206 amino acids. All members of the VEGF family stimulate cellular responses by binding to tyrosine kinase receptors (VEGFRs) on the cell surface, causing them to dimerize and activate through transphosphorylation [20].

Recently, it has been reported that hepatic fibrosis and angiogenesis develop in parallel in the liver [19, 21]. Indeed, neovessel formation has been observed in liver biopsies of cirrhosis, chronic hepatitis C, and autoimmune hepatitis [22]. Furthermore, liver fibrosis tightly correlates with angiogenesis in human liver samples [23]. Fibrosis promotes angiogenesis via the induction of VEGF from activated HSCs [24, 25]. In turn,

increased neovessel formation induced by VEGF causes fibrosis, although the underlying molecular mechanism remains undetermined. The elucidation of this mechanism would shed a new light on not only the understanding of the cross-talk between cells in the liver, but also anti-fibrotic strategies.

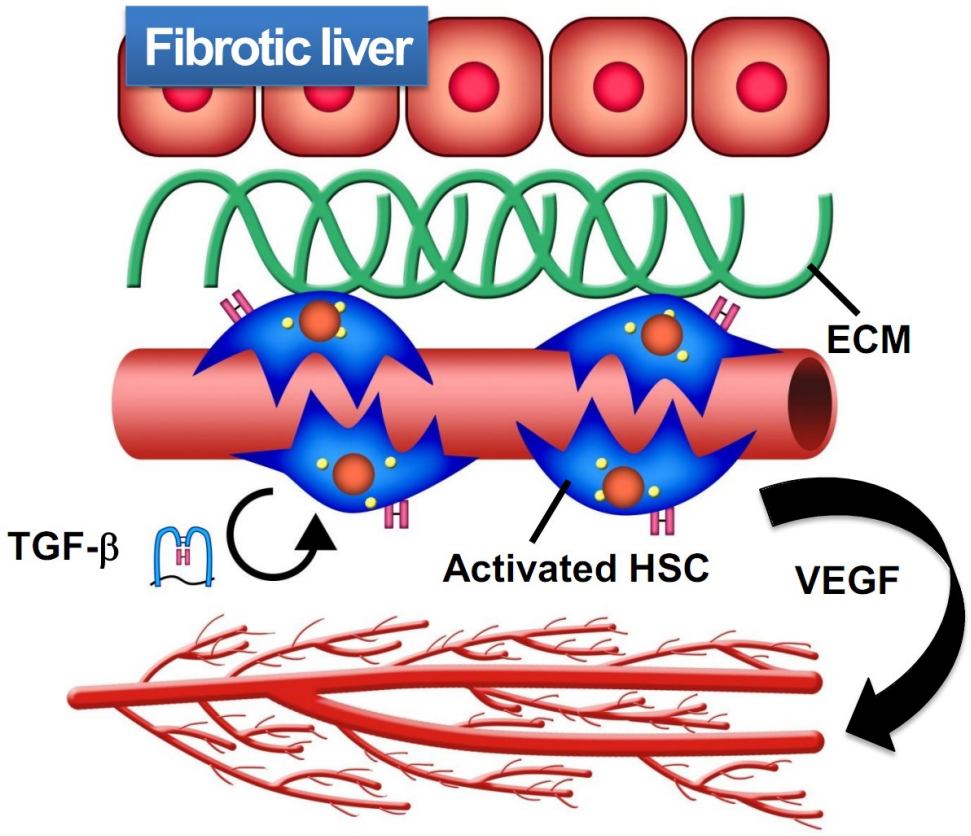


**Figure 1-5. Cross-talk between HSCs and ECs in hepatic angiogenesis and fibrogenesis**

# Chapter 2

# HCV NS3 protease enhances liver fibrosis via binding to and activating TGF-β type I receptor

## 2-1. Introduction

Viruses sometimes hijack the host cell machinery by mimicking host cell proteins. This strategy infers survival, infection, and replication advantages to the virus [26, 27], which may thereby contribute to the development of human diseases.

HCV causes liver fibrosis, a process largely mediated by the overexpression of TGF-β and collagen, although the precise underlying mechanism is unknown. The author firstly focused on the activation of TGF-β, the most potent fibrogenic cytokine.

Because the LAPs of TGF-β2 and -β3 have sequences that share partially homology with the NS3 cleavage site between NS3 and NS4A of HCV [28], the author speculated that NS3 might activate TGF-β2 and/or TGF-β3 via the proteolytic cleavage of their LAP portions. The author found, however, that NS3 DID NOT directly activate latent TGF-β2/3. Instead, it mimicked TGF-β2 and induced TGF-β signaling by binding and activating TβRI, leading to the induction of fibrogenic genes. This pathway was enhanced in the presence of an inflammatory cytokine, tumor necrosis factor (TNF)-α, as TNF-α increased the expression of TβRI. Furthermore, the author found that NS3 colocalized with TβRI on the surface of an HCV-infected hepatoma cell line, and observed direct binding between recombinant NS3 and TβRI. These phenomena were reproduced in chimeric mice transplanted with human hepatocytes that had been infected with HCV. These data suggest a novel mechanism by which HCV induces liver fibrosis.

## 2-2. Results

### 2-2-1. HCV NS3 protease exerted TGF-β mimetic activity via TβRI

To confirm whether HCV NS3 might induce the activation of latent TGF-β2, bacterially expressed recombinant NS3 (Fig. 2-1) was incubated with HEK293T cell conditioned medium after transiently overexpressing latent TGF-β2, and the concentration of active TGF-β2 in the reaction mixtures were measured by ELISA. Although the addition of NS3 increased active TGF-β2 concentrations in a dose-dependent manner, these increases were not time-dependent (Fig. 2-2). Instead, the author found that NS3 itself reacted with TGF-β2 in a dose-dependent manner, as determined by ELISA (Fig. 2-3). Next, to assess whether NS3 could induce the bioactivity of TGF-β via TβRI, and whether its activity was dependent on protease activity, the author performed a luciferase reporter assay with the TGF-β-responsive $(CAGA)_9$-luc reporter in CCL64 cells. NS3 demonstrated TGF-β mimetic activity, which was alleviated in the presence of TβRI kinase inhibitors (SB-431542 and LY-364947) (Fig. 2-4) in a dose-dependent manner (Fig. 2-5). In contrast, an NS3 protease inhibitor, VX-950 (Fig. 2-4), did not affect NS3-induced luciferase activity (Fig. 2-5). An unrelated protein with almost the same molecular weight as NS3, HLA class II histocompatibility antigen, DM α chain (HLA-DMA), as well as a carrier-free, tag-control sample, did not exert TGF-β mimetic activity, thus

demonstrating the specificity of NS3 (Fig. 2-6 and 2-7). Additionally, an anti-TGF-β2 antibody that detected NS3 in the TGF-β2 ELISA did not inhibit luciferase activity (Fig. 2-8).

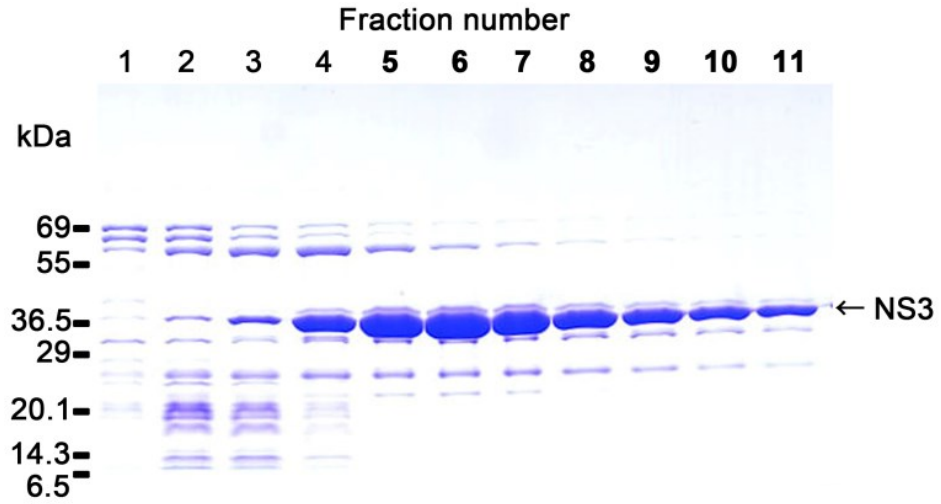


**Figure 2-1. The purification of the NS3 protein**

Bacterially expressed NS3 protein was sonicated 10 times for 30 seconds and centrifuged at 16,000 x *g* for 20 min at 4°C. The supernatant was filtrated and fractionated by a HisTrap HP column. Fraction numbers 5 to 11 were mixed and used for the subsequent assays.

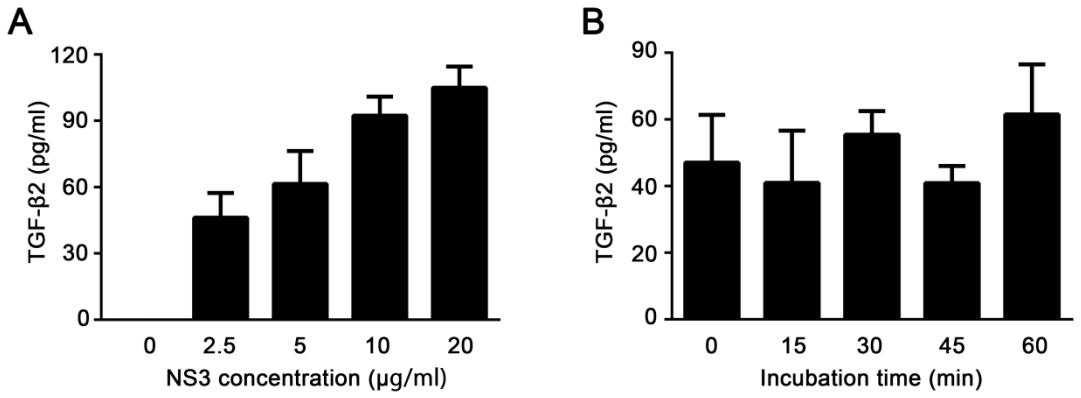


**Figure 2-2. NS3 did not activate latent TGF-β2**

(A) The indicated concentrations of recombinant NS3 protease were incubated at 37°C for 30 min with conditioned medium obtained from HEK293T cells transiently overexpressing latent TGF-β2. The reaction mixture was subjected to active TGF-β2 ELISA. (B) Ten μg/ml recombinant NS3 protease were incubated at 37°C for the indicated times with conditioned medium obtained from HEK293T cells transiently overexpressing latent TGF-β2. The reaction mixture was subjected to active TGF-β2 ELISA.

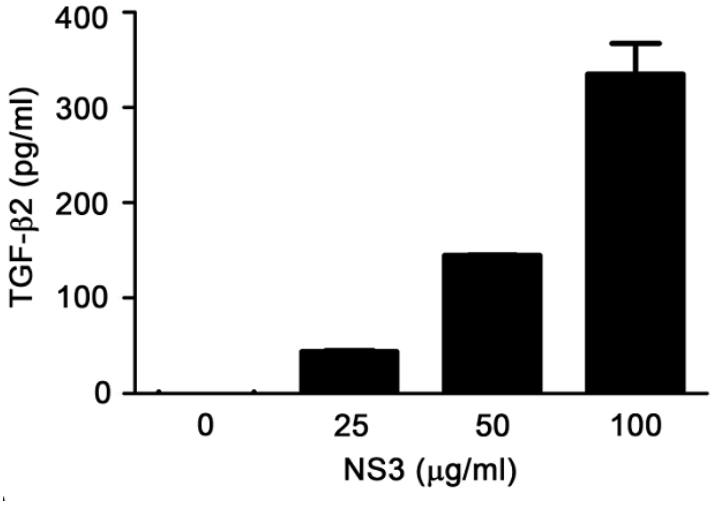


**Figure 2-3. HCV NS3 protease exerted TGF-β2 antigenicity**

The indicated concentrations of recombinant NS3 protease were used in the TGF-β2 ELISA assays.

**SB-431542**

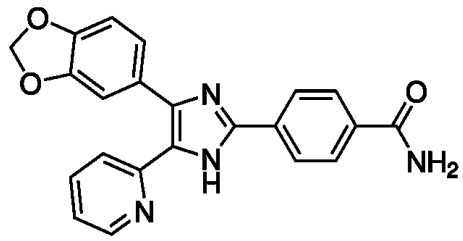

**LY-364947**

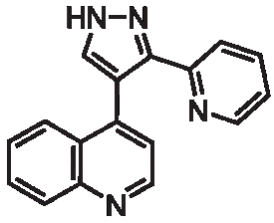

**VX-950**

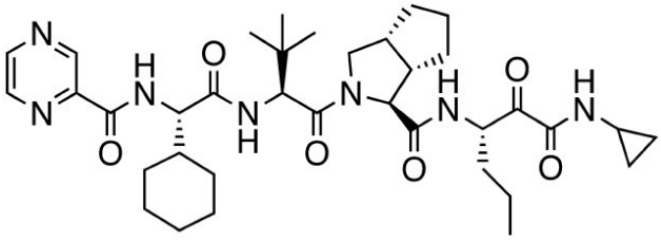

**Figure 2-4. Chemical structures of SB-431542, LY-364947, VX-950**

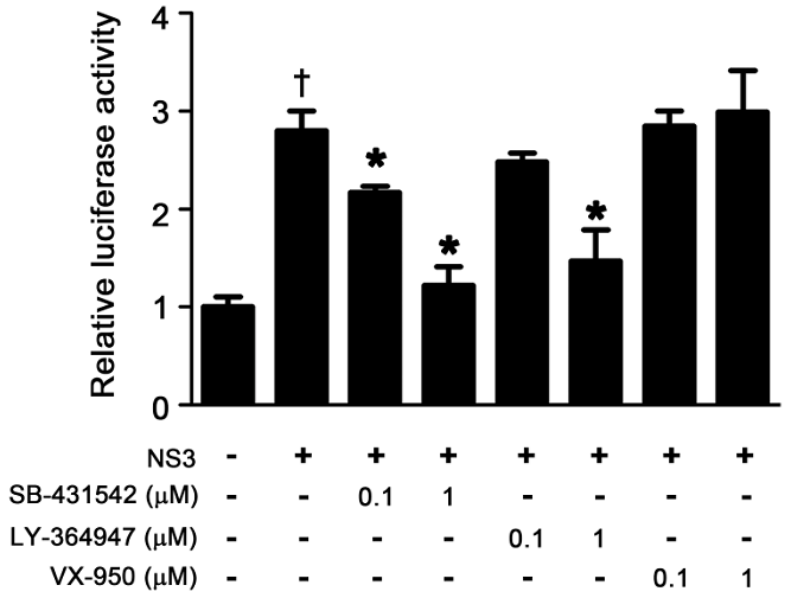


**Figure 2-5. HCV NS3 protease exerted TGF-β mimetic activity via the type I receptor**

(CAGA)$_9$-Luc CCL64 cells were stimulated with 100 μg/ml of recombinant NS3 protease for 24 hours, with or without the indicated concentration of TβRI kinase inhibitor or the NS3 protease inhibitor VX-950 (telaprevir). After 24 hours, the cells were harvested and luciferase activities were measured. †$p < 0.05$ compared with untreated control cells, *$p < 0.05$ compared with NS3-treated cells without any inhibitors. The data are shown as the mean ± SD (n=3), and representative results from three independent experiments with similar results are shown.

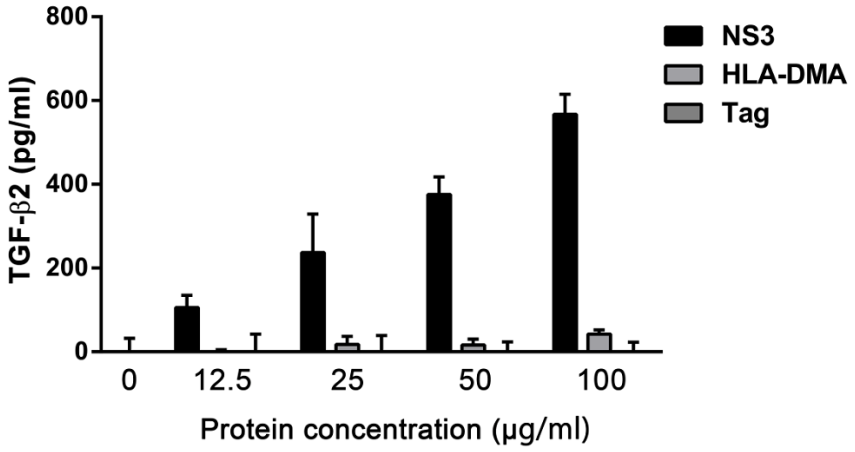


**Figure 2-6. The specific TGF-β2 antigenicity of NS3**

Recombinant NS3 protease (NS3, black bars), HLA class II histocompatibility antigen, DM α chain (HLA-DMA, light gray bars), or fractions purified from carrier-free plasmid samples (Tag control, dark gray bars) were subjected to TGF-β2 ELISA.

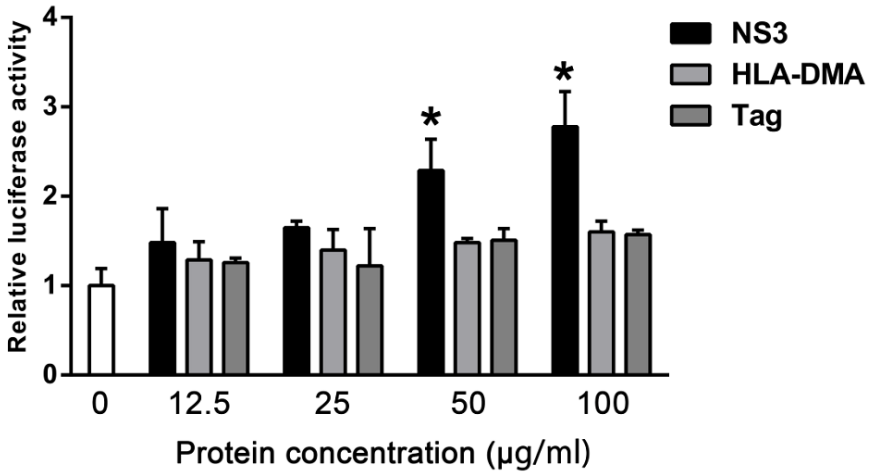


**Figure 2-7. The specific TGF-β bioactivity of NS3.**

$(CAGA)_9$-Luc CCL64 cells were stimulated with the indicated concentrations of recombinant NS3 protease, HLA-DMA, or tag control samples for 24 hours. After 24 hours, the cells were harvested and luciferase activities were measured. $^*p < 0.05$ compared with untreated control cells.

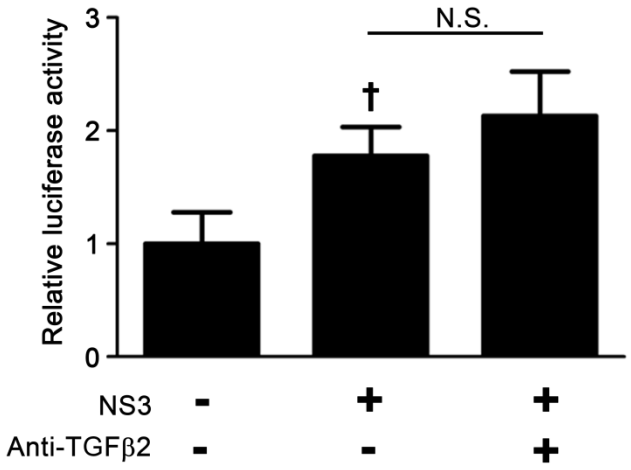


**Figure 2-8. TGF-β mimetic activity of NS3 was not inhibited by anti-TGF-β2 antibody**

(CAGA)$_9$-Luc CCL64 cells were stimulated with 100 μg/ml of recombinant NS3 protease for 24 hours, with or without anti-TGF-β2 antibody which had been used for TGF-β2 ELISA. After 24 hours, the cells were harvested and luciferase activities were measured. †$p < 0.05$ compared with untreated control cells. N.S., no significant difference. The data are shown as the mean ± SD (n=3).

**2-2-2. NS3 stimulated collagen production in hepatic cells, which was augmented by TNF-α**

The author examined the effect of NS3 on the expression of TGF-β1 and collagen α1 (I) in the human hepatic stellate cell line LX-2. Treatment with NS3 for 12 hours significantly increased both TGF-β1 (1.6-fold) and collagen α1 (I) (1.4-fold) expression in these cells (Fig. 2-9A). On the contrary, NS3 did not affect the expression of these genes in the normal hepatic cell line Hc. The pretreatment of the cells with tumor necrosis factor-α (TNF-α) enhanced increased TGF-β1 and collagen α1 (I) expression mediated by NS3 and was also accompanied by an increase in TGF-β receptor expression (Fig. 2-9B). Further increases in TβRI expression were not observed by combination treatment with TNF-α, suggesting that TNF-α increased TβRI expression, which may enhance the TGF-β mimetic activity of NS3 in these cells. Furthermore, Smad3 phosphorylation was also induced by NS3 in Hc cells that had been pretreated with TNF-α (Fig. 2-10B). A similar cooperativity between TNF-α and NS3 protease was not observed in LX-2 cells (Fig. 2-10A).

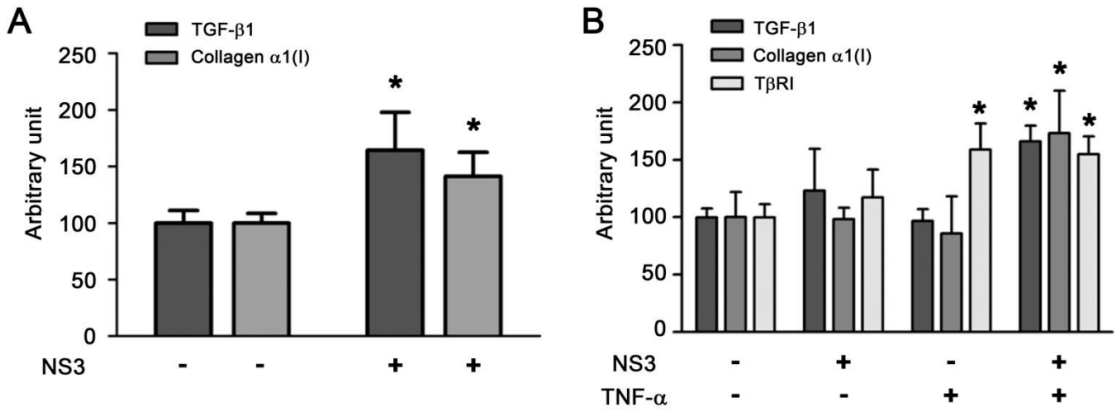


**Figure 2-9. Cooperativity between NS3 and TNF-α in the stimulation of TGF-β1, collagen α1(I), and TβRI expression.**

(A) Effect on TGF-β1 and collagen α1(I) mRNA expression in LX-2 cells. The cells were stimulated with 50 μg/ml of NS3 for 12 hours. Total cellular RNA was isolated and reverse transcribed to cDNA, and real-time PCR was performed as described in the Methods section. *$p < 0.05$ compared with untreated control cells. (B) Effect of pretreatment with TNF-α on the stimulation of expression of TGF-β1, collagen α1(I), and TβRI by NS3 protease in HC cells. Following the pretreatment of the cells with 20 ng/ml TNF-α for 12 hours, they were stimulated with 25 μg/ml NS3 for 12 hours, and mRNA expression was measured as described above. *$p < 0.05$ compared with untreated cells. The data are shown as the mean ± SD (n=3).

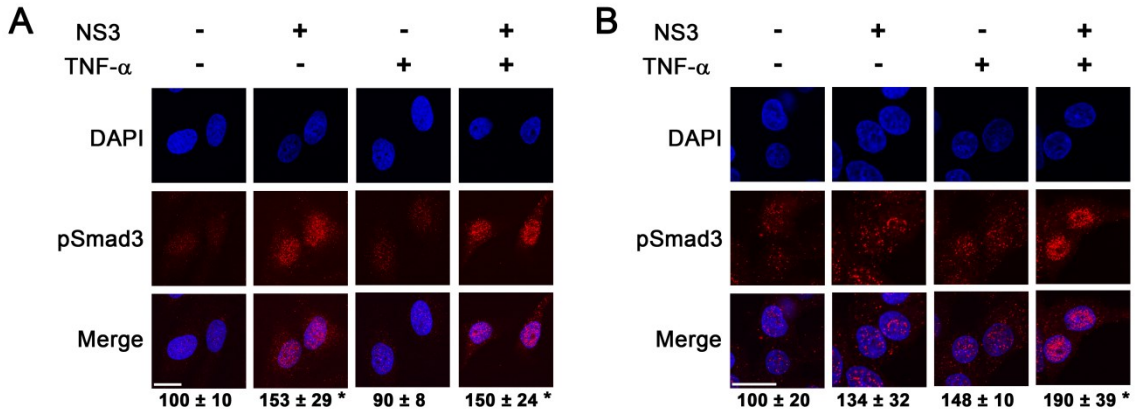


**Figure 2-10. The effect of pretreatment with TNF-α on the stimulation of phosphorylation of Smad3 by NS3 protease**

After LX-2 cells (A) and Hc cells (B) were treated with 20 ng/ml TNF-α for 12 hours and 25 μg/ml NS3 for another 12 hours, they were fixed, and immunofluorescent staining was performed as described in the Methods section. The experiments were performed in duplicate. The relative fluorescence intensities of phospho-Smad3 (% of untreated control cells) in 4 randomly selected fields from each dish were calculated with ZEN software and are shown as the mean ± SD. *$p < 0.05$ compared with untreated cells. The results are representative of three independent experiments with similar results. Scale bar, 10 μm.

### 2-2-3. Interaction between NS3 and TβRI on the surface of HCV-infected HCC cells

NS3 was immunostained on the surface of HCV-infected Huh-7.5.1 cells both with and without permeabilization. In contrast, an ER marker, calnexin, was only positive after the permeabilization of the cells (Fig. 2-11A). To examine whether NS3 that was localized to the surface of HCV-infected Huh-7.5.1 cells interacted with TβRI, the author performed co-immunostaining (Fig. 2-11B) and in situ proximity ligation assay (PLA) (Fig. 2-12) using antibodies against NS3 and TβRI. Both results showed that NS3 was colocalized and formed a complex with TβRI on the cell surface. The author also co-cultured Huh-7.5.1 infected with HCV and LX-2 cells and examined them using *in situ* PLA. However, the interaction between NS3 protease and TβRI was not observed on the surface of LX-2 cells. Furthermore, the author performed co-immunoprecipitation assays using recombinant NS3 and the extracellular domain of TβRI and TβRII. As shown in Figure 2-13, FLAG-tagged NS3 bound to TβRI and TβRII, whereas FLAG-tag alone failed to interact with TGF-β receptors (Fig. 2-13).

Docking simulation using the Katchalski-Katzir algorithm [(29)] predicted that NS3 interacts with TβRI at three sites, T22-S42, T76-P96, and G120-S139, in NS3 and F55-M70, I72-V85, and C86-Y99 in TβRI, respectively (Fig. 2-14, Table 1, and Fig. 2-15). The predicted binding site peptides, particularly the peptide derived from site 3, completely blocked the interaction between NS3 and TβRI in the

immunoprecipitation experiment (Fig. 2-16). Antibodies produced to these predicted binding sites within both NS3 and TβRI decreased the TGF-β mimetic activity of NS3 in $(CAGA)_9$-Luc CCL64 cells (Fig. 2-17A-C). Furthermore, the anti-NS3 antibody inhibited HCV-induced Smad3 phosphorylation (Fig. 2-18).

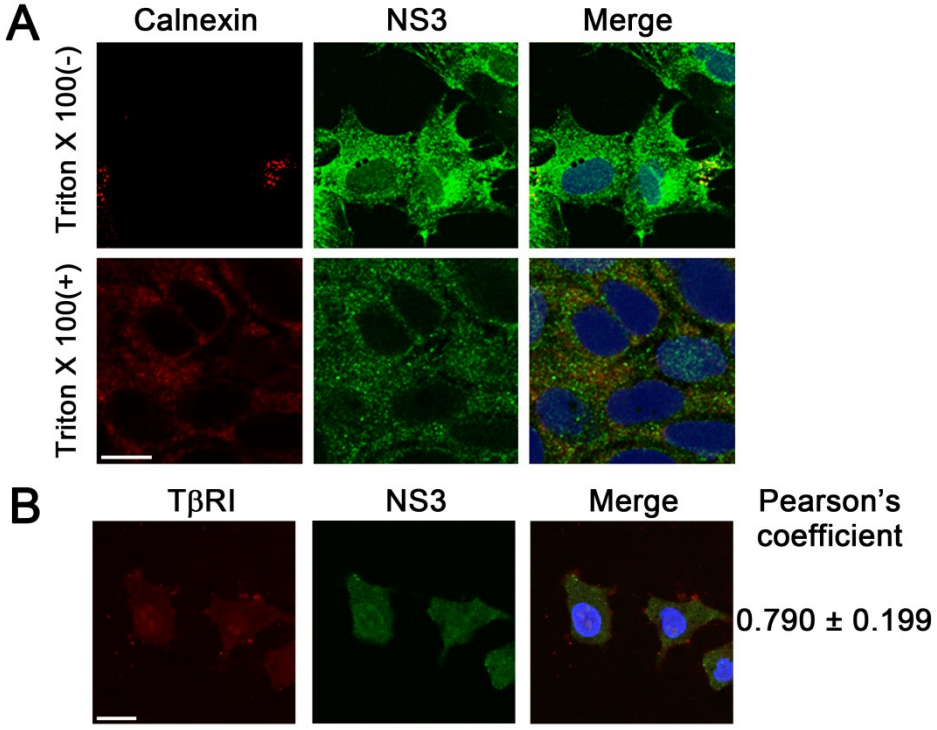


**Figure 2-11. NS3 protease colocalized with TβRI on the surface of HCV-infected cells**

(A) The detection of NS3 protease on the surface of HCV-infected Huh-7.5.1 cells. The cells were fixed, followed ± by permeabilization with Triton-X 100, and then stained with DAPI (blue), anti-NS3 antibody (green), and anti-calnexin antibody (red). (B) The colocalization of NS3 protease with TβRI in HCV-infected Huh7.5.1 cells. The cells were fixed and stained with DAPI (blue), anti-NS3 antibody (green), and anti-TβRI antibody (red), as described in the Methods section. Pearson's colocalization coefficient values were obtained from 4 randomly selected fields using the ZEN software. Scale bar, 10 μm. The results are shown as the mean ± SD and are representative of three independent experiments with similar results.

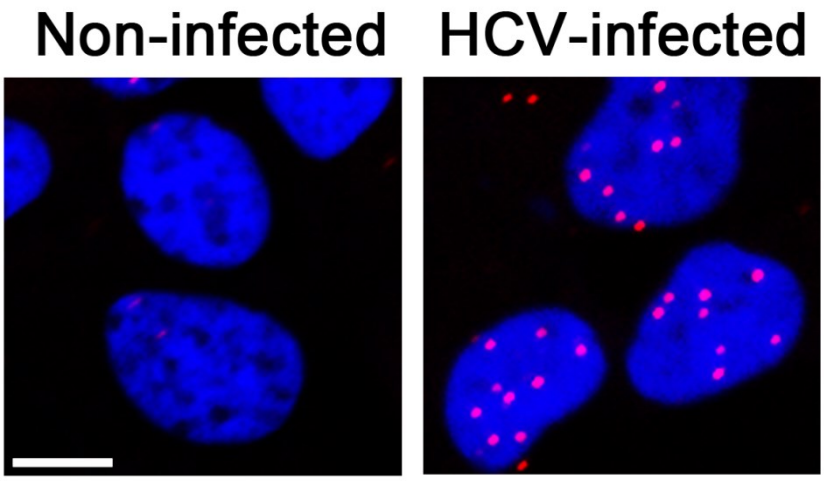


**Figure 2-12. The detection of NS3-TβRI proximity by in situ PLA in HCV-infected Huh-7.5.1 cells**

The red dots indicate interaction between NS3 protease and TβRI, and the nuclei were stained with DAPI. Scale bar, 10 μm.

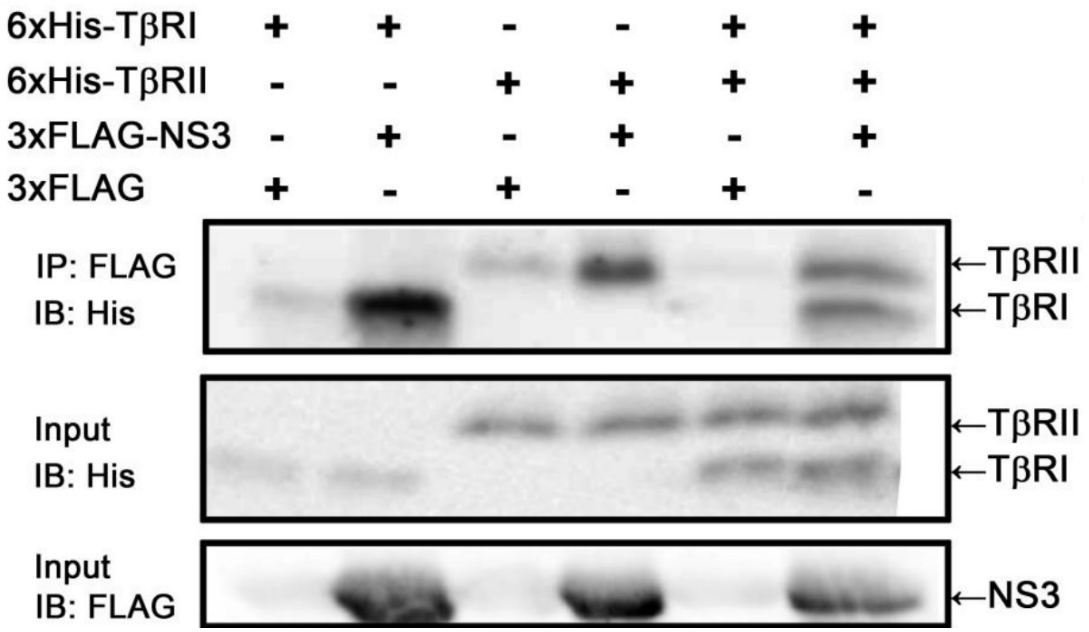


**Figure 2-13. The physical interaction of NS3protease with TβRI and TβRII**

FLAG-tagged NS3 protease was incubated with 6xHis-tagged TβRI and/or TβRII and immunoprecipitated. The coprecipitated proteins were visualized by immunoblotting using anti-His antibody. The gels were run under the same experimental conditions.

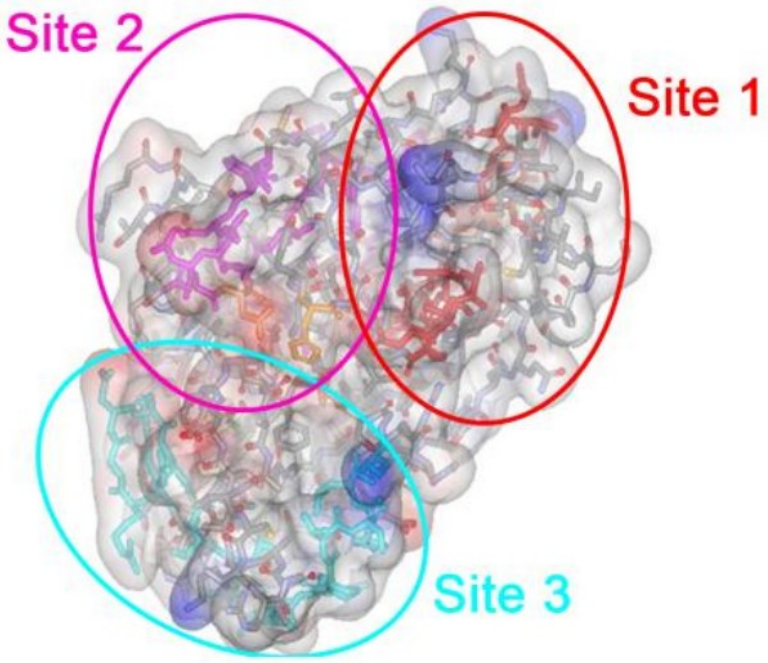


**Figure 2-14. The structural overview of the NS3 protease**

The indicated colored amino acids (site 1, red; site 2, magenta; and site 3, cyan) show the important residues within the putative binding sites to TβRI, and the sequences are presented in Table 1.

| | NS3 protease | TβRI |
|---|---|---|
| Site 1 | [22] TGRDKNQVEGEVQVVSTATQS [42] | [55] FVSVTETTDKVIHNSM [70] |
| Site 2 | [76] TNVDQDLVGWPAPPGARSLTP [96] | [72] IAEIDLIPRDRPFV [85] |
| Site 3 | [120] GDNRGSLLSPRPVSYLKGSS [139] | [86] CAPSSKTGSVTTTY [99] |

The underlined letters denote the putative contact residues.

The superscript numbers denote amino acid positions.

**Table 1. The amino acid sequences of predicted binding sites between NS3 protease and TβRI.**

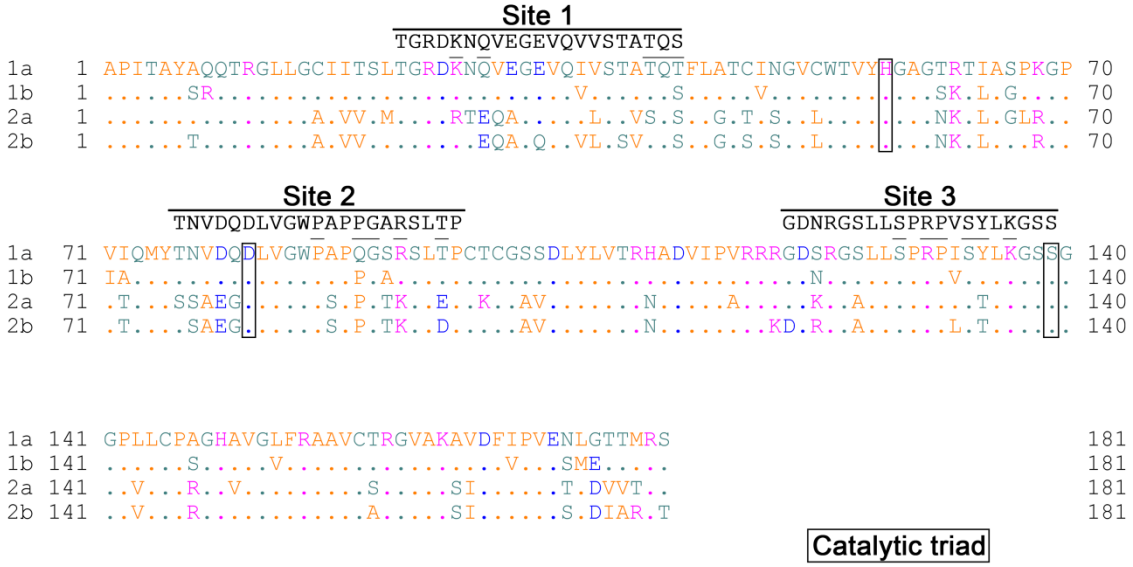


**Figure 2-15. Amino acid alignment of HCV NS3 protease (1-181) of various genotypes, including 1a (H77 strain), 1b (HCV-N strain), 2a (JFH-1 strain), and 2b (MA strain)**

The multiple sequence alignments were generated by GENETYX version 11 (Genetyx, Tokyo, Japan). The following amino acid sequences of HCV NS3 protease (1-181) of various genotypes were obtained from GenBank: AAB67036.1 for genotype 1a (H77 strain); AAB27127.1 for genotype 1b (HCV-N); AEJ86546.1 for genotype 2a (JFH-1 strain); and BAB08107.1 for genotype 2b (MA strain). The dots indicate amino acids that are identical to the top sequence. Sites 1, 2, and 3 are the predicted binding sites with TβRI. The amino acids enclosed in square boxes indicate the catalytic triad of NS3 protease. The predicted binding sites, particularly site 3, were conserved among genotypes.

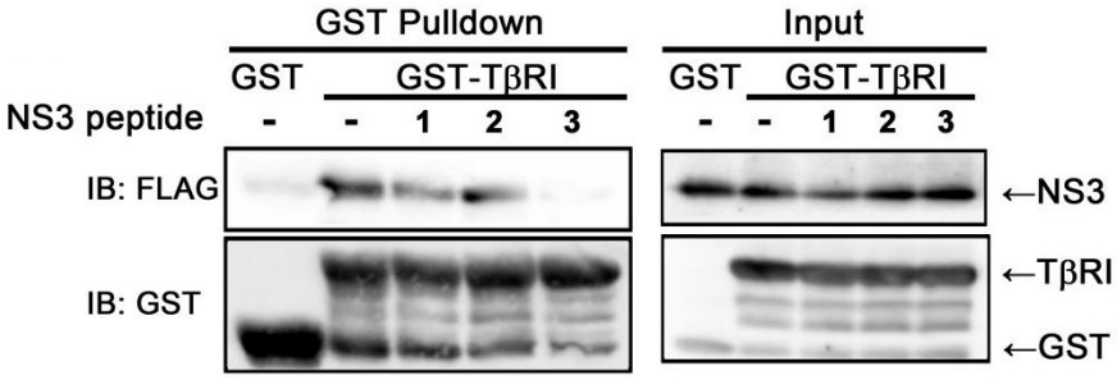


**Figure 2-16. Inhibition by the NS3 peptides of physical interaction between NS3 protease with TβRI**

GST-TβRI or GST was pre-incubated with indicated peptides for 3 hours, then mixed with 3xFLAG-NS3, followed by pull-down with Glutathione-Sepharose. Bound proteins were eluted with 20 mM glutathione and subjected to immunoblotting with anti-FLAG antibody (NS3 protein) or anti-GST antibody (GST-fusion proteins) (left panel). Input samples before pull-down were also visualized by immunoblotting (right panel). The gels have been run under the same experimental conditions.

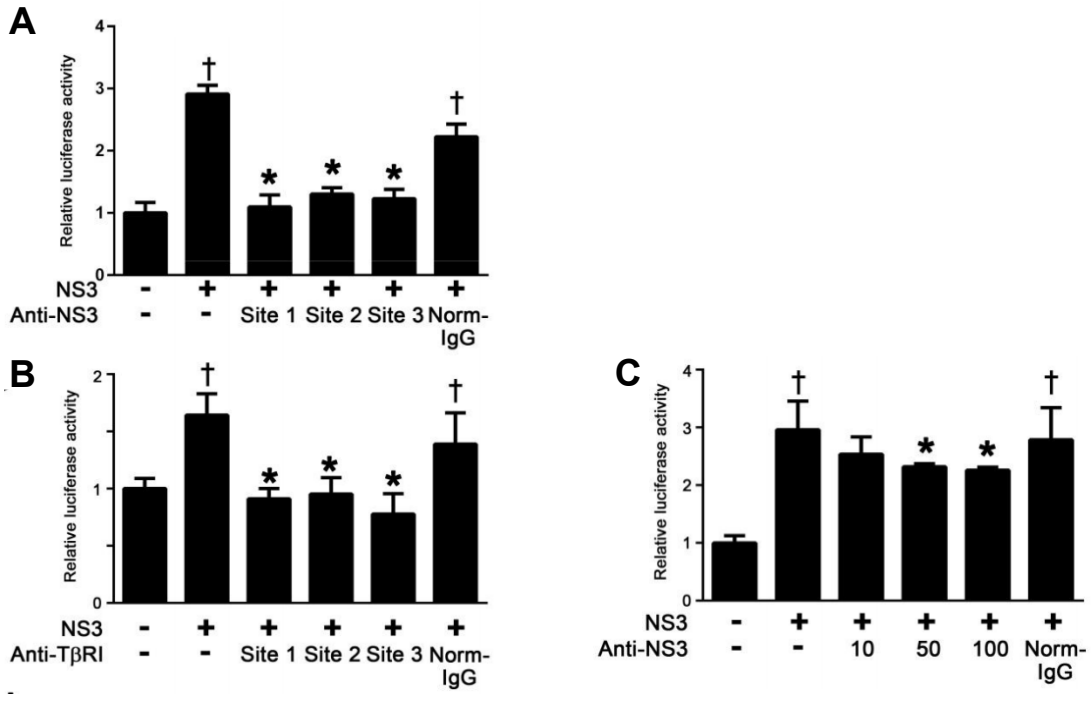


**Figure 2-17. TGF-β mimetic activity of NS3 was inhibited in the presence of either anti-NS3 antibody or anti-TβRI antibody predicted binding sites**

(CAGA)$_9$-Luc CCL64 cells were incubated with 50 μg/ml of recombinant NS3 protease for 24 hours, with or without the indicated concentrations of either anti-NS3 polyclonal antibodies against the predicted binding sites of TβRI (A), or anti-TβRI polyclonal antibodies against predicted binding sites of NS3 (B), and anti-NS3 monoclonal antibody against predicted binding site 3 of TβRI (C). The cells were harvested and luciferase activities were measured as described before. Normal mouse IgG (Norm-IgG) was used as a negative control. The data are shown as the mean ± SD. †$p < 0.05$ compared with untreated control cells, *$p < 0.05$ compared with NS3-treated cells without any antibodies. Representative results from three independent experiments with similar results are shown.

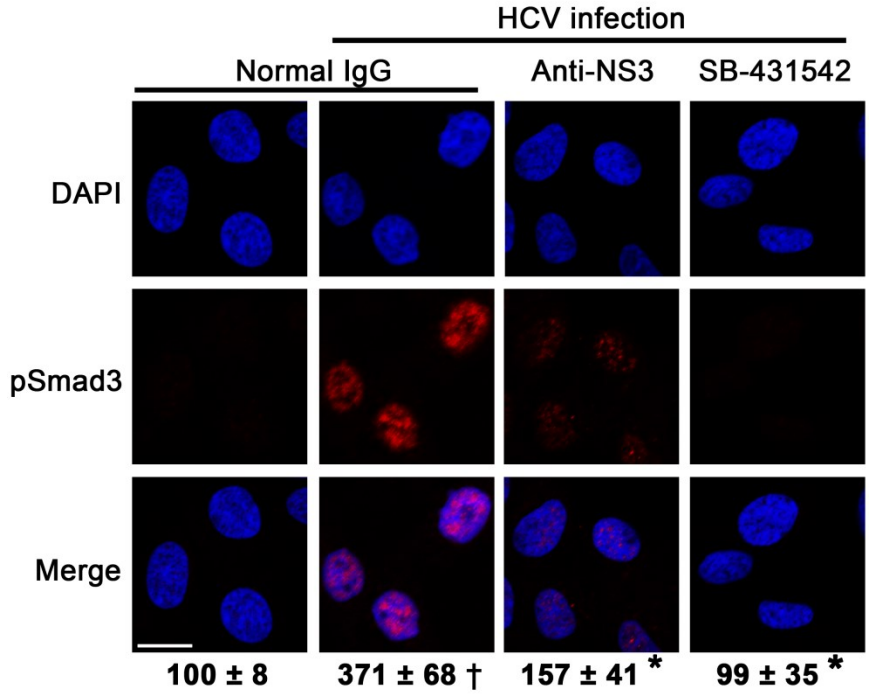


**Figure 2-18. Inhibition of HCV-induced Smad3 phosphorylation in Huh-7.5.1 cells by anti-NS3 antibody**

The cells were fixed and stained with DAPI and anti-phospho-Smad3 antibody (pSmad3), as described in the Materials and Methods section in this chapter. SB-431542, a TβRI kinase inhibitor, was used as a positive control. The relative fluorescence intensities (% of non-infected control cells) from 4 randomly selected fields from each dish were calculated by the ZEN software and are shown as the mean ± SD. †$p < 0.05$ compared with non-infected cells. *$p < 0.05$ compared with HCV-infected normal IgG-treated cells. The results are representative of two independent experiments with similar results. Scale bar, 10 μm.

### 2-2-4. Anti-NS3 antibody prevented liver fibrosis in HCV-infected chimeric mice

To test our hypothesis that NS3 exerts TGF-β mimetic activity, thereby causing liver fibrosis, the author examined whether the anti-NS3 antibody could prevent liver fibrosis in HCV-infected human hepatocyte-transplanted chimeric mice. The anti-NS3 antibody significantly prevented hepatic collagen accumulation in the mice (Fig. 2-19) and decreased the mRNA expression of both TGF-β1 and collagen α1 (I) (Fig. 2-20A-B). There was no significant change in the serum levels of human albumin and HCV RNA during treatment with the anti-NS3 antibody (Fig. 2-21).

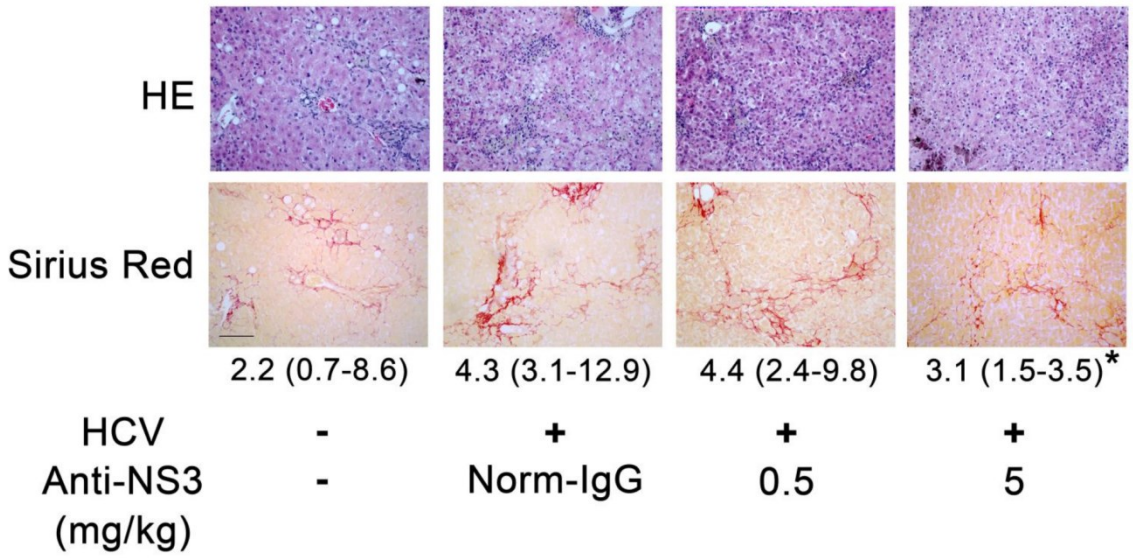


**Figure 2-19. Anti-NS3 antibody prevented collagen accumulation in the HCV-infected chimeric mice**

Paraffin sections were prepared from the livers of HCV-infected chimeric mice 16 weeks after HCV inoculation, and stained with hematoxylin and eosin (HE, upper panels) and Sirius Red (lower panels). An anti-NS3 antibody was administered at the indicated doses, and normal mouse IgG (Norm-IgG) was administered at a dose of 5 mg/kg. For each group, the median ratios in Sirius Red positive/total area (%) from 6 randomly selected fields are shown, with the range in parentheses. $^{*}p < 0.05$ compared with HCV-infected mice without anti-NS3 antibody. Scale bar, 100 μm. The representative results from 6 randomly selected fields are shown.

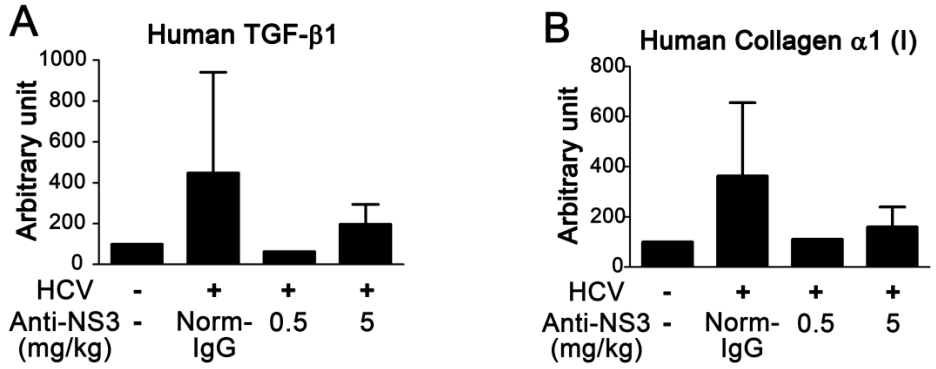


**Figure 2-20. Hepatic mRNA expression in HCV-infected chimeric mice**

Total RNA was isolated from the livers of these mice and reverse transcribed to cDNA, and real-time PCR was performed as described in the Methods section to quantitate the expression of human TGF-β1 expression (A) and human collagen α1 (I) (B). The data are shown as the mean ± SD, and representative results from two independent experiments with similar results are shown.

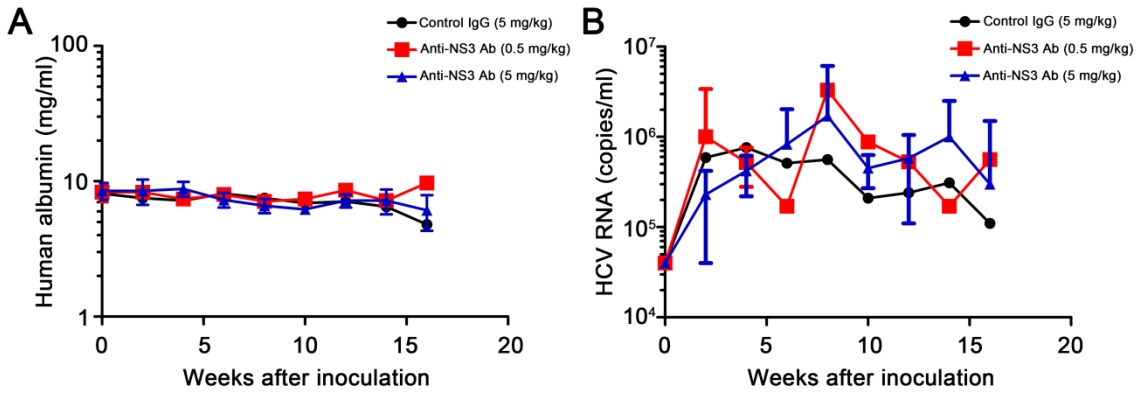


**Figure 2-21. Anti-NS3 antibody did not affect human albumin concentrations in chimeric mouse blood and HCV RNA levels in HCV-infected chimeric mice.** Blood samples were collected once two weeks from the orbital veins at the indicated times. (A) Human albumin concentrations were measured using an Alb-II kit (Eiken Chemical, Tokyo, Japan) according to the manufacturer's instructions. The data are shown as the mean ± SD. (B) Total RNA was extracted from serum using a SepaGene RV-R RNA extraction kit (Sanko Junyaku, Tokyo, Japan). The amplification of HCV RNA was performed using TaqMan EX RT-PCR Core Reagents (Life Technologies, Carlsbad, CA). The primer sequences used are as follows: HCV RNA forward: 5'- CGG GAG AGC CAT AGT GG-3'; reverse: 5'- AGT ACC ACA AGG CCT TTC G-3'; and probe: 5'-FAM- CTG CGG AAC CGG TGA GTA CAC-TAMRA-3'. The data are shown as the geometric mean ± SD.

## 2-3. Discussion

Several groups have studied the molecular mechanisms by which HCV induces liver fibrosis and have reported the following: (i) HCV core protein activates the TGF-β1 promoter via the MAPK pathway in core protein-expressing human hepatocellular carcinoma HepG2 cells [30]; (ii) recombinant core protein upregulates the expression of fibrogenic genes in the human hepatic stellate cell line LX-2 via the toll-like receptor 2 [31] and the obese receptor [32]; and (iii) NS3 protease induces TGF-β1 production in NS3-overexpressing human hepatoma Huh-7 cells [33]. Our data show that NS3 protease mimics TGF-β2 and directly exerts its activity, at least in part, via binding to and activating TβRI, thereby enhancing liver fibrosis. The following experiments should be carried out in the future: effect of NS3 on TβRI phosphorylation, the expression of TGF-β2, TGF-β3, and other TGF-β responsive genes, such as plasminogen activator inhibitor-1, a tissue inhibitor of metalloproteinase-1, and α-SMA, to further validate the TGF-β mimetic activity of NS3.

HCV NS3 is a chimera of helicase and serine protease, which cleaves not only the junction between NS3-4A, NS4A-4B, NS4B-5A, and NS5A-5B for viral polyprotein processing, which is essential to the viral lifecycle, but also the toll-interleukin-1 receptor domain-containing, adaptor-inducing β-interferon, and mitochondrial

antiviral signaling protein, which results in the disruption of innate immune responses [28, 34]. An NS3 protease inhibitor, telaprevir, which was approved by the FDA in 2011, has been used in triple combination therapy with the current standard treatment of PEGylated interferon and ribavirin [35]. Telaprevir did not inhibit TGF-β mimetic activity assessed with a $(CAGA)_9$-luciferase reporter gene assay (Fig. 2-5), suggesting that the TGF-β mimetic activity of NS3 is independent of its protease activity.

Much interest has centered on the fact that extraordinarily high concentrations of NS3 protease, up to 100 μg/ml, could exist in proximity to a TGF-β receptor. This line of inquiry led us to identify the synergism between NS3 and TNF-α, although the synergistic effect was maximal at one fourth this concentration of NS3. Serum levels of TNF-α in chronic hepatitis C patients are known to be significantly higher than those in healthy subjects [36, 37]. The author showed that TNF-α increased the susceptibility of cells to NS3 by enhancing the expression of TβRI, thereby further increasing the levels of profibrogenic genes (Fig. 2-9). Various hepatic cell lines expressed different levels of TβRI, and there appeared to be a threshold in the level of TβRI that enabled cells to produce collagen mRNA upon stimulation with NS3. In particular, Hc cells expressed levels of TβRI below this predicted threshold (Fig. 2-22). Consistent with our findings, carbon tetrachloride has recently been reported to induce acute liver injury, specifically significant liver fibrosis with inflammation, in transgenic mice expressing the full-length HCV polyprotein [38].

The author documented the colocalization of NS3 and TβRI on the cell surface of HCV JFH-1-infected Huh-7.5.1 cells (Fig. 2-11 and 2-12). The results of co-immunoprecipitation and in situ PLA studies supported this conclusion. In future studies, the author intends to use mutagenesis experiments of the predicted binding site and competition assays using NS3 and TGF-β in $(CAGA)_9$-Luc CCL64 cells to determine the mechanism of NS3 and TβRI binding. However, at present, how NS3 is released to the extracellular milieu remains to be elucidated. One possibility is that NS3 leaks passively from injured hepatocytes, as is the case for alanine aminotransferase and aspartate aminotransferase. Another possibility is that NS3 is secreted from HCV-infected cells via the Golgi complex. A recent report showed that nonstructural protein (NS) 1 of the dengue virus (DENV) and West Nile virus (WNV) is secreted from DENV- and WNV-infected cells through the Golgi complex following expression in association with the endoplasmic reticulum. Like HCV, these viruses are also members of the family *Flaviviridae* [39].

Zhang *et al*. identified antibodies against NS3 in the serum of chronic hepatitis C patients and suggested that extracellular NS3 may be present in such cases [40]. However, it remains unclear whether the concentration of HCV NS3 is as high as in our in vitro experiments. Although DENV NS1 has been reportedly detected at high levels (up to 50 μg/ml) in the serum of DENV-infected patients [41], further study is warranted to determine the serum or tissue NS3 concentrations in patients with

chronic hepatitis C.

In this study, the author generated polyclonal and monoclonal anti-NS3 antibodies that block the NS3-TβRI interaction. All anti-NS3 and anti-TβRI polyclonal antibodies generated against the predicted binding sites almost completely blocked TGF-β mimetic activity of NS3. This finding was likely due to steric hindrance by these antibodies or a requirement of binding at all three sites for signal transduction by NS3. The monoclonal antibody is a powerful tool that can be used to explore our working hypothesis that NS3 enhances liver fibrosis via the TGF-β receptor in vivo.

In conclusion, the author demonstrated for the first time that HCV NS3 protease serves as a novel TGF-β receptor ligand and enhances liver fibrosis. This phenomenon might be beneficial to the virus, as TGF-β signals suppress host immunity. Our results provide elucidation regarding the molecular mechanism by which HCV induces liver fibrosis.

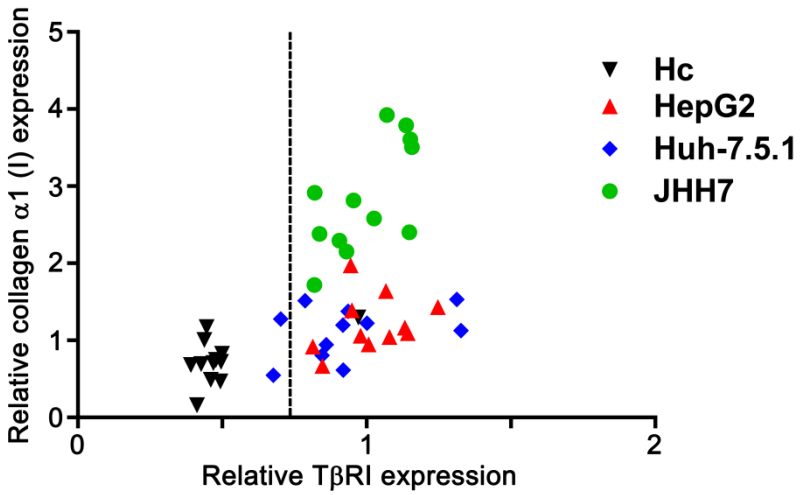


**Figure 2-22. Correlation between collagen α1 (I) and TβRI expression in hepatic cell lines.**

Various human hepatic cell lines, including Hc, HepG2, Huh-7.5.1, and JHH7, were treated with or without 25 μg/ml NS3 for 12 hours, and the mRNA expression levels of TβRI, collagen α1 (I), and glyceraldehyde-3-phosphate dehydrogenase (GAPDH) were measured as described in the Materials and Methods section in this chapter. The relative expression levels of TβRI (*x*-axis) and collagen α1 (I) (*y*-axis) were normalized to GAPDH. The broken line shows the predicted threshold.

## 2-4. Materials and Methods

### Materials

SB-431542 and LY-364947 were purchased from Sigma-Aldrich (St. Louis, MO). Recombinant human TNF-α was purchased from R&D systems, Inc. (Minneapolis, MN). Anti-NS3 antibody and anti-calnexin antibody were purchased from Abcam (Cambridge, UK). Anti-TβRI antibody and anti-phospho-Smad3 antibody were purchased from Santa Cruz Biotechnology (Santa Cruz, CA) and Immuno-Biological Laboratories (Gunma, Japan), respectively. Anti-Flag M2 antibody and anti-His antibody were purchased from Sigma (St. Louis, MO). Anti-NS3 antibodies and anti-TβRI antibodies against predicted binding sites were provided by the BioMatrix Research Institute (Chiba, Japan).

### Cell culture

$(CAGA)_9$-Luc CCL64 cells were kindly provided by Prof. Hideaki Kakeya (Kyoto University, Kyoto, Japan), the hepatic stellate cell line LX-2 [42] was kindly provided by Prof. Norifumi Kawada (Osaka City University, Osaka, Japan), and the human hepatoma cell line Huh-7.5.1 [43] were maintained in Dulbecco's modified Eagle's medium (DMEM) supplemented with 10% fetal bovine serum, penicillin, and streptomycin. HC cells [44], a normal human hepatocyte cell line purchased from Cell

Systems (Kirkland, WA), were cultured in CS-C complete medium (Kirkland, WA).

**Protein preparation**

The gene-encoding N-terminal histidine-tagged NS3 protease was cloned into the pET32a (+) vector and expressed in *Escherichia coli* (KRX) by isopropyl-β-thiogalactopyranoside induction. The protein was purified by affinity chromatography in a HisTrap HP column (GE Healthcare, Waukesha, WI) and was dialyzed in 20 mM Tris-HCl buffer (pH 8.0) containing 500 mM NaCl, 20 μM $ZnCl_2$, and 1 mM Tris (2-carboxyethyl) phosphine. p3xFLAG-2 was constructed from pFLAG2 (Sigma) by inserting a synthetic oligonucleotide between the *Hin*dIII and *Eco*RI sites. The cDNA sequence-encoding NS3 protease (1-181) was amplified by PCR using pcDNA3-MEF-NS3-4A as a template and was cloned into the *Eco*RI and *Xho*I sites of p3xFLAG-2. The cDNA sequences encoding the extracellular domain of human TβRI (30 to 115) and TβRII (15 to 136) were amplified by PCR and were cloned into the *Bam*HI and *Xho*I sites of pQE30 (Qiagen) or pGEX-6P-1 (GE Healthcare). p3xFLAG-NS3 was introduced into the *E. coli* strain BL21(DE3) harboring pG-KJE8 (TAKARA). pQE-TβRI and pQE-TβRII were introduced into *E. coli* M15[pREP4] harboring pG-KJE8. pGEX-TβRI and pGEX-TβRII were introduced into *E. coli* BL21 harboring pG-KJE8 (TAKARA). The proteins were expressed overnight at 20°C after induction with 0.5 mM isopropyl

β-thiogalactopyranoside. After being harvested, the cells were lysed in a buffer solution (20 mM Tris-HCl, pH 7.5, 150 mM NaCl, 20 μM $ZnCl_2$) by sonication on ice. The lysate was clarified by centrifugation at 4°C, 10,000 x *g* for 20 min.

**Enzyme-linked immunosorbent assay (ELISA)**

TGF-β2 ELISA was performed using a TGF-β2 Emax® Immune Assay System ELISA kit (Promega, Madison, WI) according to the manufacturer's instructions.

**Luciferase assay**

The mink lung epithelial cell line CCL64, which stably expressed $(CAGA)_9$-MLP-luciferase and contained nine copies of a Smad-binding CAGA box element upstream of a minimal adenovirus major late promoter ($2x10^4$ cells/well) [(45)], was seeded into 96-well plates. The next day, the medium was replaced with fresh medium containing 0.1% bovine serum albumin, and the cells were cultured for an additional 24 hours. The cells were extracted with lysis buffer, and luciferase activity was measured by a Luciferase Assay System (Promega, Madison, WI) according to the manufacturer's instructions.

**Real-time RT-PCR**

The isolation of total RNA and real-time RT-PCR were performed as described

previously [46]. Briefly, total RNA was extracted using the RNeasy mini kit (Qiagen, Valencia, CA) according to the manufacturer's protocols. RNA (0.5 μg) was reverse transcribed to cDNA using the PrimeScript® RT Master Mix (Takara Bio Inc., Shiga, Japan). The mRNA expression levels were determined using real-time PCR. Real-time PCR was performed with the Thermal Cycler Dice® Real Time System, using the SsoAdvanced™ SYBR® Green Supermix (Bio-Rad Laboratories, Hercules, CA) and normalized to GAPDH mRNA expression. The primer sequences used were as follows: human TGF-β1 forward: 5'-ACT ATT GCT TCA GCT CCA CGG A-3', reverse: 5'-GGT CCT TGC GGA AGT CAA TGT A-3'; human collagen α1 (I) forward: 5'-ACG AAG ACA TCC CAC CAA TC-3', reverse: 5'-AGA TCA CGT CAT CGC ACA AC-3'; human GAPDH forward: 5'-GGA GTC AAC GGA TTT GGT-3', reverse: 5'-AAG ATG GTG ATG GGA TTT CCA-3'; and human TβRI forward: 5'-CTT AAT TCC TCG AGA TAG GC-3', reverse: 5'-GTG AGA TGC AGA CGA AGC-3'.

**Immunofluorescence staining**

The cells were grown on eight-well chamber slides or glass bottom dishes and were incubated with HCV virion for 24 hours at 37°C. The cells were washed with phosphate buffered saline (PBS), fixed with 4% paraformaldehyde for 10 min at room temperature, and permeabilized with 0.1% Triton X-100 for 20 min at room

temperature (RT). After blocking with 3% bovine serum albumin (BSA)/10% normal goat serum/PBS for 30 min, the cells were incubated with primary antibodies for 2 hours, followed by incubation with secondary antibodies for 30 min at RT. For detecting NS3 and TβRI on the cell surface, the cells were fixed without permeabilization after incubation with the secondary antibodies. After being washed with PBS, the cells were mounted with Vectashield DAPI mounting medium (Vector Laboratories, Inc., Burlingame, CA) and observed under the Zeiss LSM 700 laser scanning confocal microscope. For quantitative fluorescence analyses, the intensity of phosphorylated Smad3 and the colocalization of NS3 and TβRI (Pearson's colocalization coefficient values) in each panel were calculated with ZEN software.

**Proximity ligation assay (PLA)**

HCV-infected Huh-7.5.1 cells were fixed with 4% paraformaldehyde for 10 min at room temperature and subjected to in situ PLA using a Duolink in situ red starter kit (Olink Bioscience, Uppsala, Sweden) according to the manufacturer's instructions. Briefly, cells were blocked and incubated with primary antibodies against NS3 and TβRI, followed by incubation with the PLA probes, which were secondary antibodies (anti-mouse and anti-rabbit) conjugated to oligonucleotides. DNA ligase was added to enable the formation of circular DNA strands when the PLA probes were in close proximity. This step was followed by incubation with oligonucleotides and

polymerase for rolling circle amplification [47]. Texas red-labeled oligonucleotides, which hybridize to the amplified products, were used for visualization. The cells were observed under a Zeiss LSM 700 laser scanning confocal microscope.

**Immunoprecipitation and immunoblotting**

Anti-FLAG M2 affinity beads were pretreated with 5% BSA in 20 mM Tris-HCl, pH 7.5, 150 mM NaCl overnight. Isotype control IgG was bound to Protein G PLUS-Agarose (Santa Cruz) pretreated with 5% BSA in 20 mM Tris-HCl, pH 7.5, 150 mM NaCl. Cell lysates with 3xFLAG or 3xFLAG-NS3 (2 mg protein) were incubated with 50 μl of the beads (10% slurry) at 4°C for 3 hours. The beads were then washed three times with the lysis buffer and incubated with lysates containing 6xHis-TβRI or 6xHis-TβRII (0.5 mg protein) at 4°C overnight. The bound proteins were eluted with the SDS-PAGE sample buffer after washing four times with the lysis buffer and then were subjected to SDS-PAGE (15% acrylamide) followed by transfer onto a PVDF membrane (Pall). The proteins were then visualized using anti-His tag HRP DirectT (MBL, 1/5000) or anti-FLAG BioM2 antibody (Sigma, 10 μg/ml) and horseradish peroxidase-conjugated anti-biotin antibody (Cell Signaling) using the ECL Western blotting detection reagent (GE Healthcare).

**GST pull-down assay with blocking peptides**

Cell lysates with GST-TβRI or GST (0.5 mg protein) incubated with 50 μg of the peptides (NS-1, NS-2, or NS-3) on ice for 3 hours. Cell lysates with 3xFLAG-NS3 (0.3 mg) were then added and further incubated on ice for 2 hours. After centrifugation for 20 min, the supernatants were incubated with 20 μl of Glutathione Sepharose beads (10% slurry) at 4ºC for 1 hour. Beads were washed four times with 20 mM Tris-HCl, pH 7.5, 150 mM NaCl, 20 μM $ZnCl_2$. Bound proteins were eluted with 20 mM glutathione in 20 mM Tris-HCl, pH 7.5, 150 mM NaCl, and visualized by immunoblotting using anti-FLAG M2 antibody (Sigma) or anti-GST antibody (GE Healthcare). Secondary antibodies used are as follows: anti mouse IgG-HRP (Jackson), anti-goat IgG-HRP (Wako).

**In silico docking simulation**

The protein-protein docking simulation was implemented based on the geometric complementarity [29] between NS3 protease (PDB ID, 1NS3) and TβRI (PDB ID, 2PJY). Specifically, coordinates of the proteins were projected onto three-dimensional grids separated from each other at regular intervals. A surface score and an intramolecular score were assigned to each grid. This operation was conducted for both the receptor and the ligand. Next, convolution between the obtained grids was performed, the surfaces were explored exhaustively, and the

complementarities of the binding states were calculated based on the scores. Amino acid residues appearing frequently in binding states with high complementarity scores can be estimated to be residues that are highly likely to appear in the interaction with an actual receptor. Accordingly, amino acid residues with an interatomic distance of 3.8 Å or less in the putative binding states were defined as contact residues and regarded as the putative contact residues of NS3 and TβRI.

**Animal experiment**

Chimeric mice with humanized livers were generated as previously described using urokinase-type plasminogen activator (uPA)-transgenic/SCID mice [(48)]. All mice were transplanted with frozen human hepatocytes obtained from a single donor. All animal experiments were approved by RIKEN Institutional Animal Use and Care Administrative Advisory Committees and were performed in accordance with RIKEN guidelines and regulations. Infection, extraction of serum samples, and euthanasia were performed under isoflurane anesthesia. Male chimeric mice (12- to 14-week old) were intravenously injected with 100 μl HCV J6/JFH-1 strain ($1x10^8$ copies/ml). Four weeks after HCV inoculation, anti-NS3 antibodies against predicted binding sites with the TβRI receptor were administered at doses of 0.5 mg/kg of body weight (BW) or 5 mg/kg of BW twice a week for twelve weeks. Normal mouse IgG was administered at a dose of 5 mg/kg of BW as a control. When the animals were

euthanized, the livers were either fixed with 4% paraformaldehyde for histological analysis or frozen immediately in liquid nitrogen for mRNA isolation.

**Staining of liver tissue sections**

The liver tissues were fixed in 4% paraformaldehyde and embedded in paraffin, and tissue sections (6 μm in thickness) were prepared with a Leica sliding microtome (Leica Microsystems, Nussloch, Germany). The liver tissue sections were deparaffinized, rehydrated, and incubated for 5 min with a drop of proteinase K (Dako Envision) in 2 mL of 50 mM Tris-HCl buffer (pH 7.5) at RT. The liver tissue sections were stained with Mayer's hematoxylin solution (Muto Chemicals) and 1% eosin Y solution (Muto Chemicals). Sirius Red, which results in a red staining of all fibrillar collagen, was used to evaluate fibrosis. Briefly, the liver sections were stained with 0.05% Fast Green FCF (ChemBlink, Inc. CAS: 2353-45-9) and 0.05% Direct Red 80 (Polysciences, Inc. CAS: 2610-10-18) in saturated picric acid (Muto Chemicals) for 90 min at RT. The ratios of Sirius Red positive/total area (%) from 6 randomly selected fields were measured for each group using WinROOF software (Mitani Corp., Tokyo, Japan).

**Statistics**

Statistical analysis was performed using one-way analysis of variance, followed by Dunnett's post-hoc test. A two-tailed Student's *t*-test was used to evaluate differences between the two groups. The Kruskal-Wallis test followed by Dunn's post-hoc test was used for multiple comparisons of Sirius Red positive areas.

# Chapter 3

# Neovessel formation enhances liver fibrosis via providing with latent TGF-β to HSCs

## 3-1. Introduction

Liver fibrosis, which is a common feature of almost all chronic liver diseases, is caused by the excessive accumulation of ECM proteins, including collagen. Akita *et al.* previously reported that latent TGF-β is activated by PLK, which is bound to GPI-anchored uPAR on the cell surface and released by phosphatidylinositol-specific phospholipase C (PI-PLC) [(9)]. Kojima *et al.* demonstrated that PLK cleaves LAP between R58 and L59 during liver fibrosis [(49)]. After cleavage, the N-terminal side LAP degradation products ending at R58 (R58 LAP-DPs) remain within the ECM of the liver tissues through LTBP, serving as a footprint for the generation of active TGF-β. They produced a specific antibody (anti-R58 antibody) that detects a neoepitope at the cutting edge of R58 LAP-DPs [(49)].

Recent studies have reported that hepatic angiogenesis and fibrogenesis occur in parallel in liver diseases, such as hepatitis, hepatic cirrhosis and liver cancer [(21, 50)], and that anti-angiogenic compounds such as sorafenib (Nexavar), a multi-kinase inhibitor approved for the treatment of liver cancer, can attenuate liver fibrosis [(51)]. Sahin *et al*. showed that VEGF transgenic mice with increased serum VEGF concentrations have augmented liver fibrosis [(24)]. However, the underlying molecular mechanism by which the overproduction of VEGF induces liver fibrosis has not yet been demonstrated.

In the current study, the author explored the hypothesis that latent TGF-β derived from increased populations of LSECs might be transferred to the surface of HSCs and activated, resulting in acceleration of HSC activation and that enhanced liver angiogenesis might have an impact on liver fibrosis.

## 3-2. Results

### 3-2-1. Simultaneous induction of hepatic angiogenesis and fibrogenesis by the injection of VEGF into mice.

VEGF administration to the mice increased the number of cellular infiltrations, endothelial cells (CD31 staining, 3.6-fold at 20 μg VEGF/kg of BW), and active HSCs (α-SMA staining, 7.6-fold at 20 μg VEGF/kg of BW), accompanying an increase in the Sirius red-positive area (4.3-fold at 20 μg VEGF/kg of BW), in a dose-dependent manner (Fig. 3-1A and B). Furthermore, significant correlations were observed among the positive areas of CD31, α-SMA, and Sirius red, suggesting that VEGF simultaneously induces angiogenesis and fibrogenesis in the liver (Fig. 3-2). The hepatic hydroxyproline levels were also increased 5-fold at 20 μg VEGF/kg of BW (Fig. 3-3).

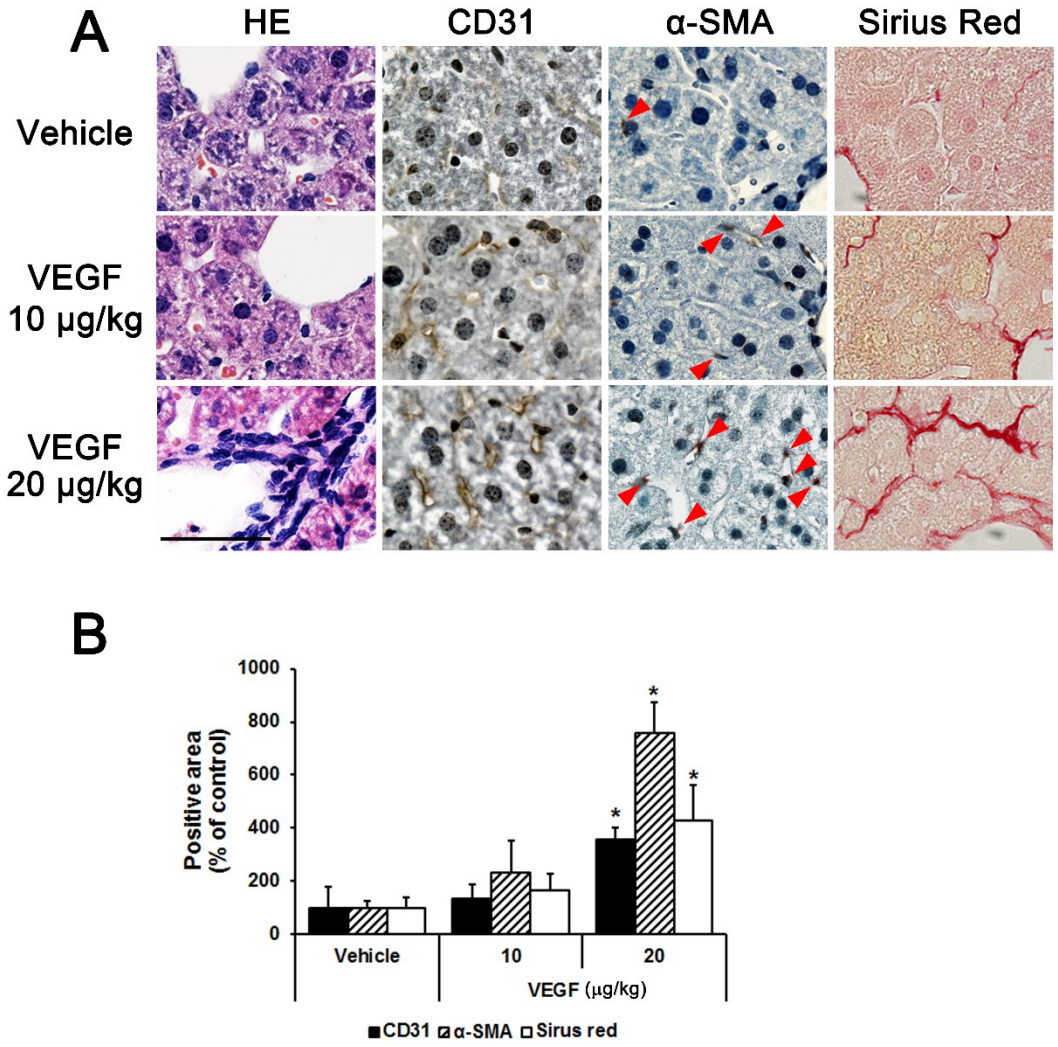


**Figure 3-1. VEGF simultaneously induced angiogenesis and fibrogenesis in the liver**

Saline (100 μl/mouse/day) without and with recombinant VEGF at the indicated doses were injected for 10 days into the tail vein of 10-week-old C57BL/6 mice (n=3). Livers were removed after the animals were euthanized. (A) Liver tissue sections were prepared and stained with HE, antibodies for CD31 and α-SMA, and Sirius red, as described in the Materials and Methods section. Scale bar is 50 μm. (B) CD31, α-SMA and Sirius red-positive areas (%) were quantitated as the average ± SD (n=3) in the bar graphs. *$p < 0.05$ compared with vehicle-treated mice.

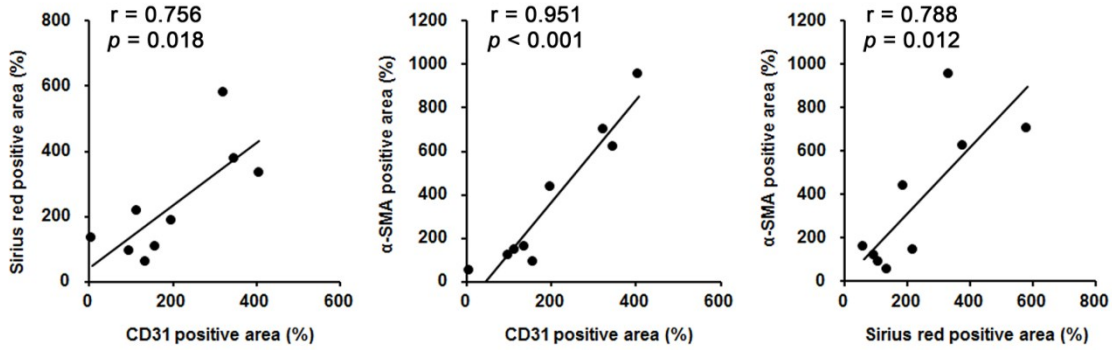


**Figure 3-2. Correlations between endothelial marker (CD31) and fibrotic markers (Sirius red and α-SMA) in VEGF-treated mouse livers.**

Quantitated positive areas for CD31 and Sirius red-positive area (left panel), CD31 and α-SMA-positive area (center panel), and Sirius red- and α-SMA-positive area (right panel) in VEGF-treated mouse livers were plotted.

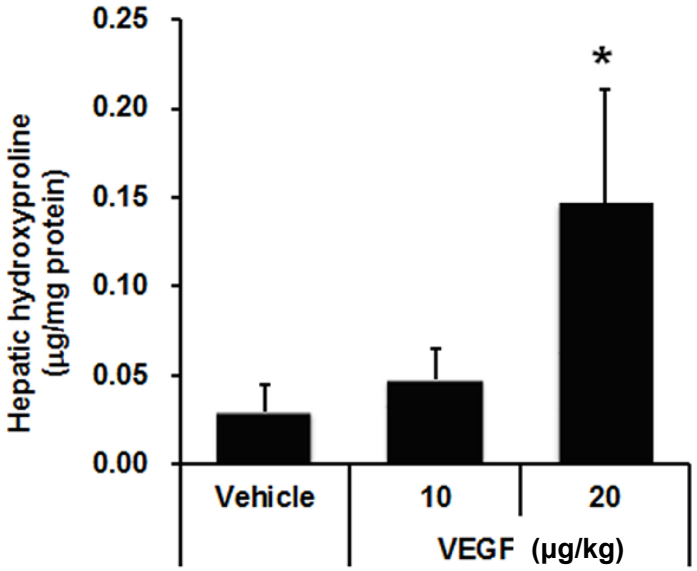


**Figure 3-3. The liver hydroxyproline levels in VEGF-treated mice**

Saline (100 μl/mouse/day) without and with recombinant VEGF at the indicated doses were injected for 10 days into the tail vein of 10-week-old C57BL/6 mice (n=3). Livers were removed after the animals were euthanized. The data are shown as the mean ± SD. *$p < 0.05$, compared with vehicle-treated mice.

### 3-2-2. The enhancement of the activation of HSCs with VEGF-treated LSEC CM via TGF-β

The author investigated the molecular mechanism by which VEGF induces hepatic fibrosis in mice using primary cell culture systems. As assessed by the lack of increase in the α-SMA levels, a marker of activated HSCs, isolated primary HSCs were not activated directly by VEGF following 5 days of treatment at 100 and 200 ng/ml, concentrations that are almost equivalent to the blood concentration of VEGF in the in vivo experiment (Fig. 3-4). VEGF also did not affect the mRNA expressions of TGF-β1, PLK, and uPAR (Fig. 3-5). VEGF enhanced latent TGF-β1 concentration (1.1-fold at 200 ng/ml VEGF) in LSEC CM (Fig. 3-6) and mRNA expressions of TGF-β1 (2.4-fold at 200 ng/ml VEGF), PLK (2.1-fold at 200 ng/ml VEGF), and uPAR (1.8-fold at 200 ng/ml VEGF) in LSECs (Fig. 3-7). HSCs were activated via incubation with recombinant TGF-β1 (100 pg/ml) and LSEC CM, the latter of which was blocked by incubation with neutralizing antibodies against TGF-β1 (Fig. 3-8).

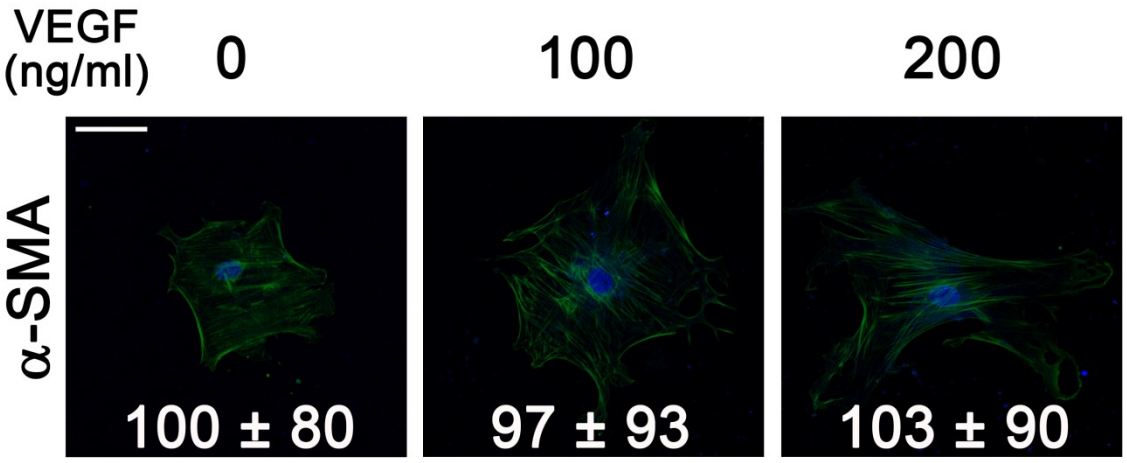


**Figure 3-4. VEGF did not directly activate HSCs**

Primary HSCs were cultured in 24-well plates. Starting in the next day, HSCs were incubated with 2% FBS DMEM in the absence or presence of the indicated concentrations of recombinant VEGF. Cells were fixed and stained with anti-α-SMA antibody, as described in the Materials and Methods section. The relative fluorescence intensities (% of untreated control cells) are shown as the mean ± SD. Scale bar, 100 μm.

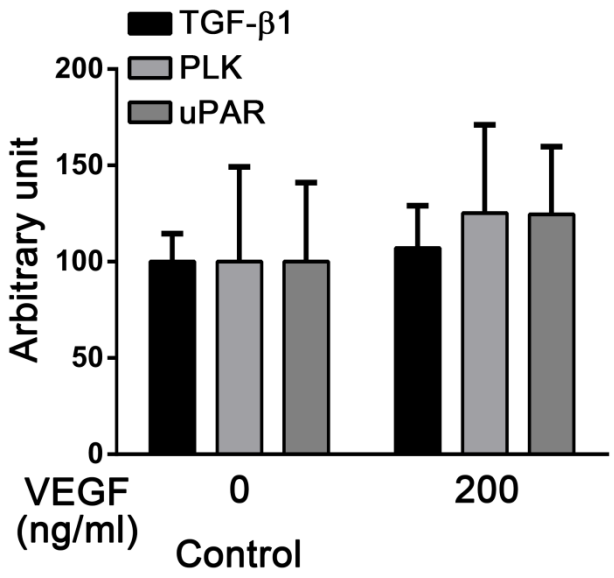


**Figure 3-5. VEGF did not affect the expressions of TGF-β1, PLK, and uPAR in HSCs**

Primary HSCs were cultured in 24-well plates. Starting in the next day, HSCs were incubated with 2% FBS DMEM in the absence or presence of the indicated concentrations of recombinant VEGF. The mRNA expression levels of TGF-β1, PLK, and uPAR were measured using real-time RT-PCR as described in the Materials and Methods section. The data are shown as the mean ± SD.

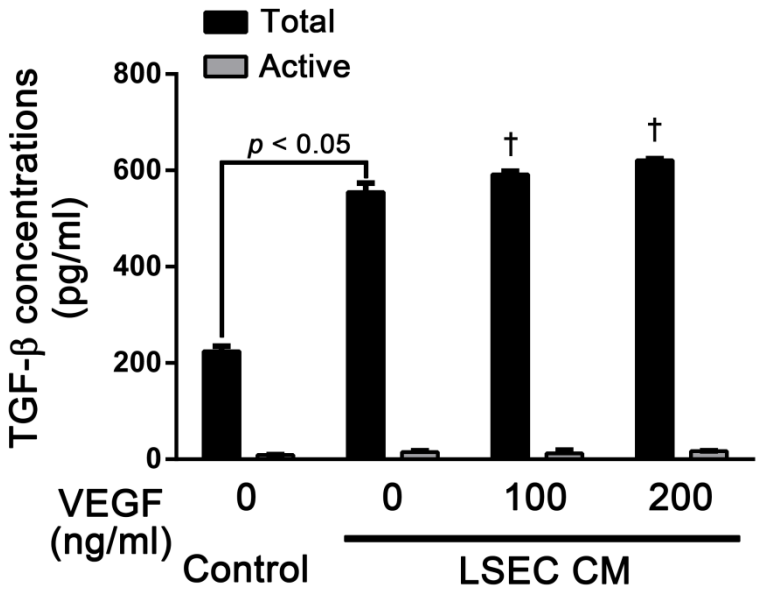


**Figure 3-6. Total/active TGF-β concentrations in VEGF-treated LSECs**

Primary LSECs were incubated with 2% FBS DMEM/F12 in the presence or absence of the indicated concentrations of recombinant VEGF for 24 hours. Total/active TGF-β1 levels in the media were measured as described in the Materials and Methods section. The data are shown as the mean ± SD. †$p < 0.05$ compared with untreated control cells.

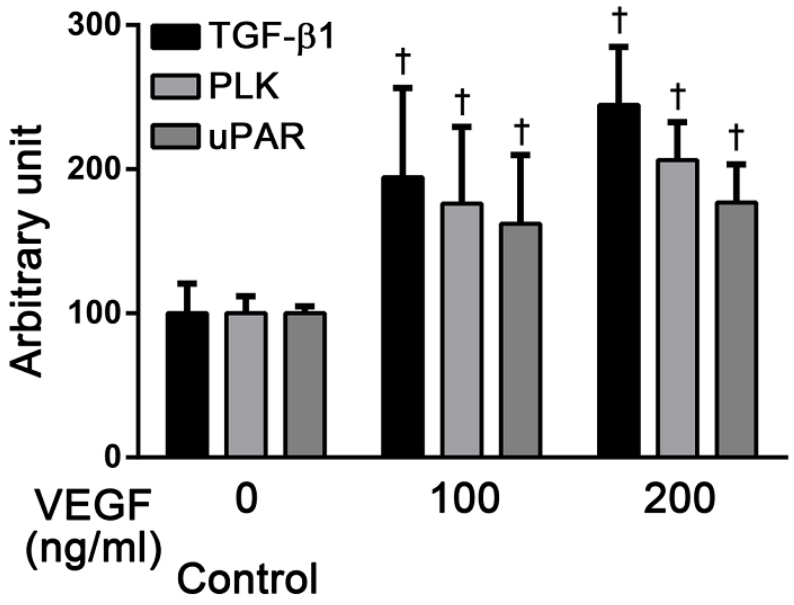


**Figure 3-7. VEGF enhanced the expressions of TGF-β1, PLK, and uPAR in LSECs**

Primary LSECs were incubated with 2% FBS DMEM/F12 in the presence or absence of the indicated concentrations of recombinant VEGF for 24 hours. The mRNA expression levels of TGF-β1, PLK, and uPAR were measured using real-time RT-PCR as described in the Materials and Methods section. The data are shown as the mean ± SD.

†$p < 0.05$ compared with untreated control cells.

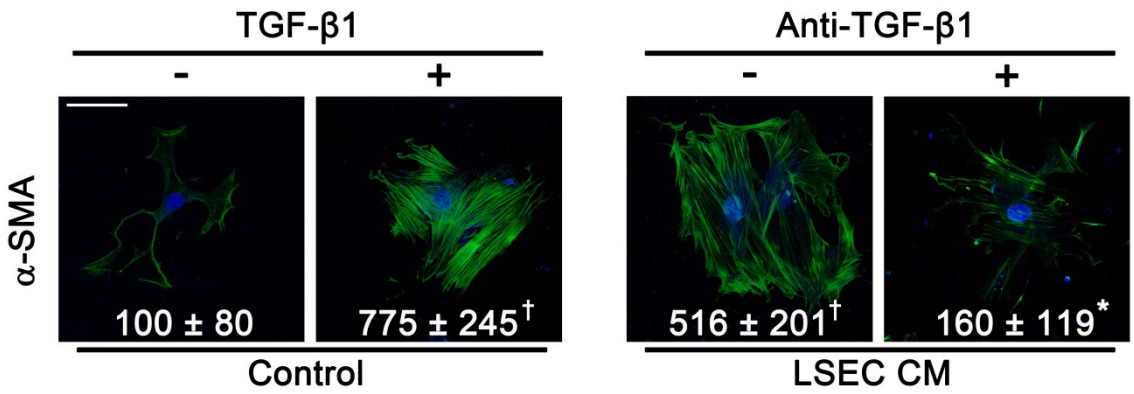


**Figure 3-8. LSEC CM enhanced HSC activation via TGF-β**

Primary HSCs were cultured in 24-well plates. Starting in the next day, HSCs were incubated with 2% FBS DMEM in the absence or presence of TGF-β1 (100 pg/ml), and LSEC CM in the absence or presence of neutralizing anti-TGF-β1 antibody (2.5 μg/ml) for 5 days. Cells were fixed and stained with anti-α-SMA antibody, as described in the Materials and Methods section. The relative fluorescence intensities (% of untreated control cells) are shown as the mean ± SD. †$p < 0.05$ compared with untreated control cells, *$p < 0.05$ compared with LSEC CM-treated control cells. Scale bar, 100 μm.

### 3-2-3. Latent TGF-β secreted from LSECs is activated by PLK on the surface of HSCs

Given the ELISA and bioassay results, we found that primary LSECs secreted only 2.5% of TGF-β in the active form during 24 hours incubation (Fig. 3-6), and that the active TGF-β concentrations in LSEC CM were slightly higher than those in the control medium (DMEM containing 2% FBS) (Fig. 3-6). To examine whether latent TGF-β present in LSEC CM was activated by PLK, the author cultured primary HSCs with LSEC CM either in the absence or presence of PI-PLC, which cleaves the glycosylphosphatidylinositol anchor, releases uPAR and is associated with PLK from the cell surface, or in the presence or absence of camostat mesilate (Fig. 3-9A), which is a serine protease inhibitor. The concentration of active TGF-β in the LSEC CM incubated with the HSCs was significantly reduced by simultaneous treatment with either PI-PLC or camostat mesilate (Fig. 3-9B). Similarly, LSEC CM failed to promote the activation of HSCs that had been incubated with either PI-PLC or camostat mesilate (Fig. 3-10). Furthermore, cells were stained using an R58 antibody that specifically detects LAP-DPs generated by PLK activation, which is the signature of TGF-β activation. As shown in Figure 3-10, the levels of R58 LAP-DPs were reduced by either PI-PLC or camostat mesilate. To confirm whether PLK-dependent activation might be increased along with neovessel formation in vivo, the liver sections harvested from the VEGF-administered mice were stained with

anti-R58 LAP-DPs antibody. As expected, the R58-positive area was increased with VEGF injection (Fig. 3-11).

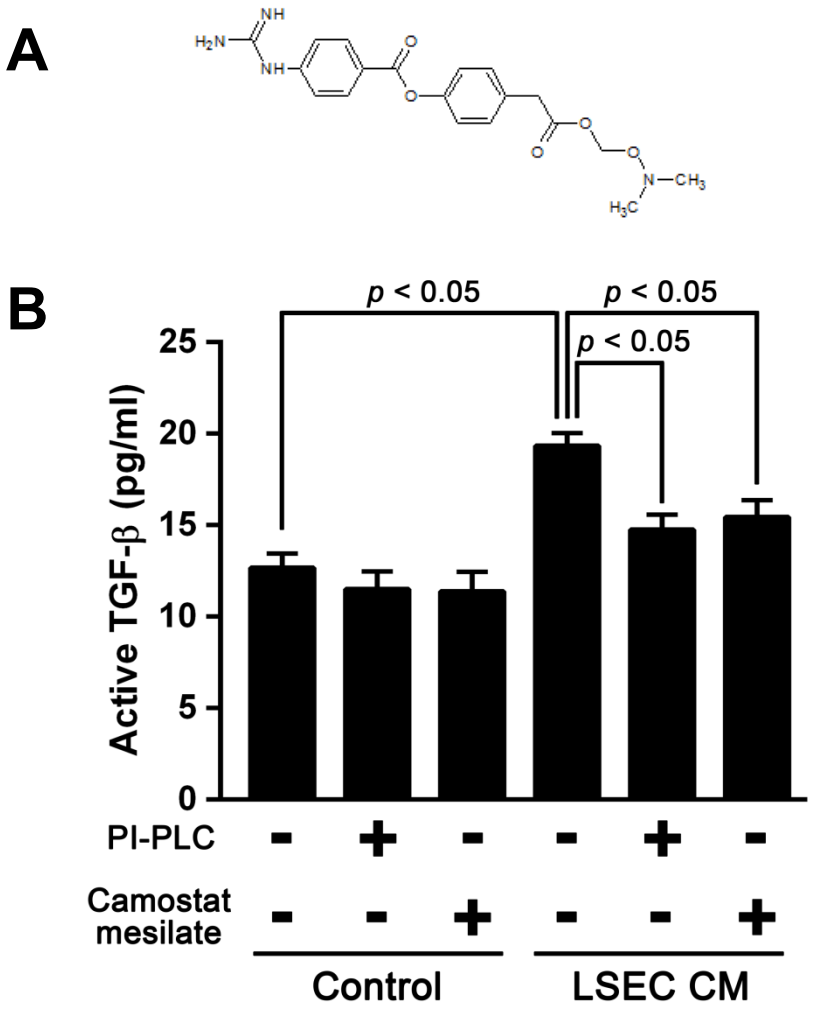


**Figure 3-9. Active TGF-β1 levels in the media of HSCs**

(A) Chemical structure of camostat mesilate, a serine protease inhibitor. (B) HSCs were incubated with 2% FBS DMEM or LSEC CM in the absence and presence of PI-PLC (0.5 U/mL) or camostat mesilate (500 μM) for 5 days. Active TGF-β1 levels in the media were assessed using the luciferase assay in $(CAGA)_9$-Luc CCL64 cells. Data are shown as the mean ± SD.

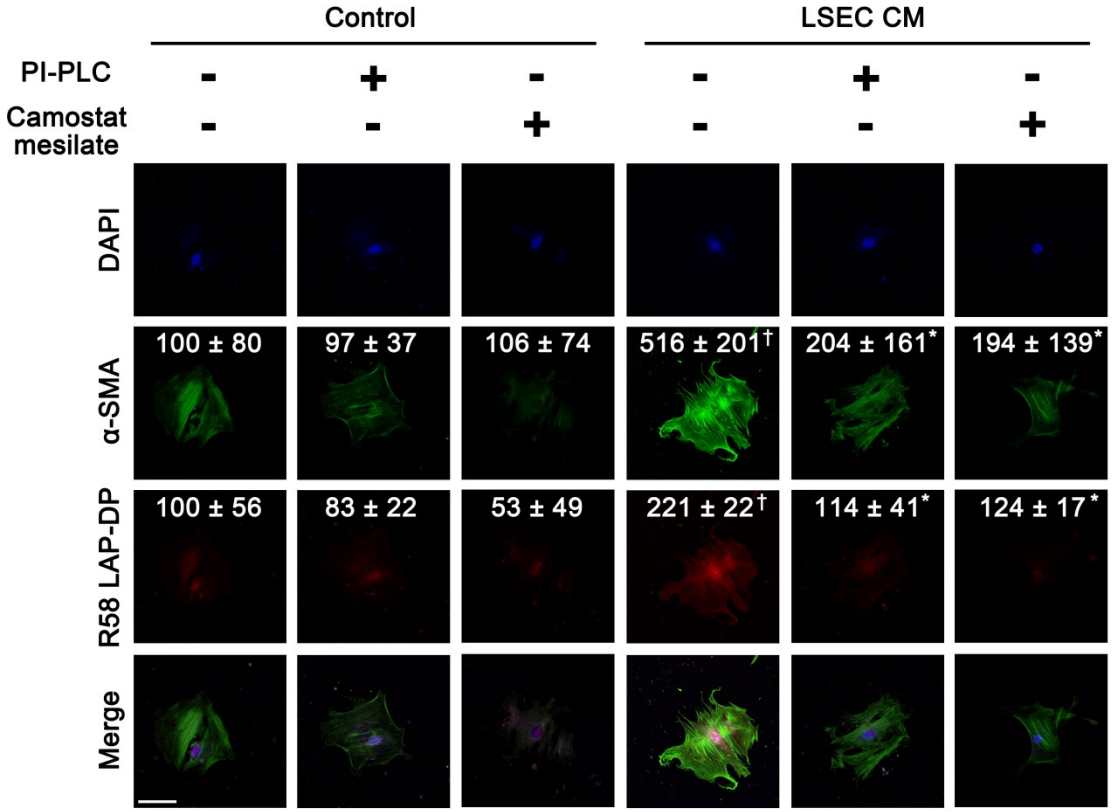


**Figure 3-10. Latent TGF-β derived from LSECs was activated on the surface of HSCs through PLK**

HSCs were incubated with 2% FBS DMEM or LSEC CM in the absence and presence of PI-PLC (0.5 U/mL) or camostat mesilate (500 μM) for 5 days. Cells were fixed and stained with anti-α-SMA (green) and anti-R58 LAP-DPs (red) antibodies, as described in the Materials and Methods section. The relative fluorescence intensities (% of untreated control cells) are shown as the means ± SD. †$p < 0.05$ compared with untreated control cells, *$p < 0.05$ compared with LSEC CM-treated control cells. Scale bar, 100 μm.

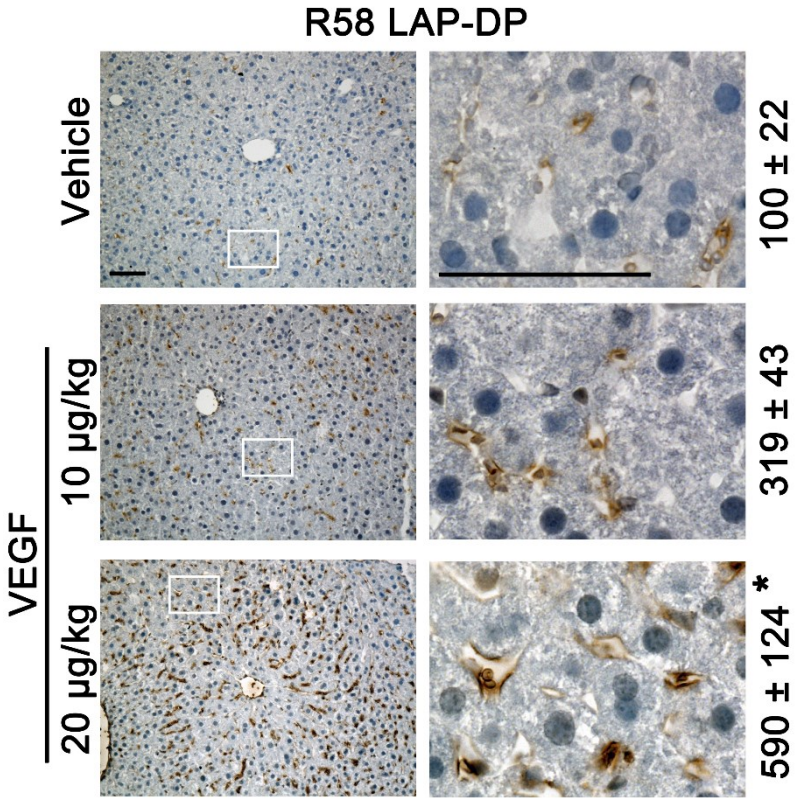


**Figure 3-11. TGF-β was activated by PLK in VEGF-administered mice liver**

The liver sections harvested from VEGF-injected mice were stained with anti-R58 LAP-DPs antibody, as described in the Materials and Methods section. The right panels show higher magnifications of the corresponding white squares in the left panels. Scale bars, 100 μm. Positive areas (%) were quantitated and shown as the means ± SD. *$p < 0.05$ compared with vehicle-treated mice.

### 3-3. Discussion

In the present study, the author addressed a role of ECs as a source of latent TGF-β, the precursor of the most fibrogenic cytokine TGF-β. We provided in vitro evidence that LSEC CM promotes the activation of quiescent HSCs via the provision of latent TGF-β and in vivo evidence that much more severe fibrosis was induced in the livers of mice that received VEGF. These data suggest that HSC activation is promoted not only via changes in the ECM, inflammatory cytokines, and oxidative stress but also secondarily via pathological angiogenesis.

We documented that TGF-β, which is secreted from LSECs as a latent form and activated on the surface of mainly HSCs rather than LSECs (compare Figs. 3-6 and 3-9), mediates enhancement in liver fibrosis, although the expressions of PLK and uPAR increased 2-fold in VEGF-treated LSECs (Fig. 3-7). Several groups have reported that VEGF enhanced the expression of urokinase-type plasminogen activator and its receptor uPAR in both bovine microvascular endothelial cells and human umbilical vein endothelial cells [(52)], enabling them matrix degradation and cell invasion [(53)], and that bradykinin production via the PLK-dependent cleavage of high molecular weight kininogen promotes angiogenesis via the upregulation of basic fibroblast growth factor [(54)]. In our study, increased PLK in LSECs might interact with HSCs and promote TGF-β activation on the surface of HSCs. At the same time, increased uPAR and PLK

in LSECs also might contribute to angiogenesis. We showed that VEGF increased the levels of hepatic CD31 by 3.6-fold and R58 LAP-DPs by 5.9-fold in mice and that VEGF enhanced latent TGF-β production and TGF-β1 mRNA expression in primary LSECs. These data also suggest that LSECs serve as the source of TGF-β for liver fibrosis.

Yoshiji *et al*. demonstrated that VEGF receptor expression increased in HSCs along with the development of fibrosis and that neutralizing anti-VEGF receptor antibody attenuated both angiogenesis and fibrogenesis in the liver, using activated HSCs [25], whereas we used quiescent HSCs. As shown in Figure 3-1, when mice were given VEGF, the number of CD31-positive endothelial cells and α-SMA-positive HSCs increased, while the Sirius red-positive area increased in a dose-dependent manner. This result might suggest that VEGF promotes the growth of LSECs, which appears to serve as a source of latent TGF-β and, as a result, increases the hepatic levels of TGF-β1, due to the increased numbers of LSECs, in the early stages of liver fibrosis. Eventually, when HSCs were activated, they started to express the VEGF receptor, respond to VEGF, and transition to a more activated state. However, the author cannot rule out the involvement of other soluble factors, such as PDGF, which is also produced from LSECs and stimulates HSC activation [19, 55]. Recent studies have reported that the inhibition of the PDGF signaling pathway by the receptor tyrosine-kinase inhibitor, imatinib, reduces portal pressure in an animal model of

cirrhosis through controlling sinusoidal remodeling and impairing the HSC coverage of the sinusoids with fewer effects on fibrogenesis [56].

Sorafenib, a multikinase inhibitor recently approved to treat unresectable hepatocellular carcinoma, has been shown to be beneficial in a model of BDL-induced cirrhosis [51, 57]. In the current study, the author has provided evidence that angiogenesis might accelerate liver fibrosis by stimulating the activation of HSCs by providing TGF-β1, which is secreted from the increased numbers of LSECs and activated on the surface of HSCs by PLK during the pathogenesis of liver diseases in mice. The anti-fibrotic effect of sorafenib might be caused by its blocking of angiogenesis. Moreover, other anti-angiogenic treatments, such as vatalanib [58] and bevacizumab [59], are now under evaluation in a clinical trial for cancer treatment. An implication of the current finding is that in addition to sorafenib, anti-angiogenic agents such as vatalanib and bevacizumab might be beneficial for anti-fibrotic therapy.

## 3-4. Materials and Methods

### Materials

Fluorescein isothiocyanate (FITC)-conjugated rat anti-mouse CD31 monoclonal antibody (Clone 390) and rat anti-mouse CD146 monoclonal antibody (Clone ME-9F1) were purchased from Millipore (Billerica, MA, USA) and Bio Legend (San Diego, CA, USA), respectively. FITC-conjugated mouse anti-α-SMA monoclonal antibody (Clone 1A4) and anti-α-SMA monoclonal antibody (Clone 1A4) were purchased from Sigma-Aldrich (St. Louis, MO, USA) and Dako (Glostrup, Denmark), respectively. Neutralizing mouse anti-TGF-β1 monoclonal antibody (Clone 9016) and sheep anti-rat IgG magnetic bead-conjugated antibody (Cat. No.110-35) were purchased from R&D Systems (Minneapolis, MN, USA) and Invitrogen (Carlsbad, CA, USA), respectively. Recombinant VEGF 165 and PI-PLC were purchased from Santa Cruz Biotechnology (Santa Cruz, CA, USA) and Sigma-Aldrich (St. Louis, MO, USA), respectively. An R58 monoclonal antibody that recognizes neo-epitope formed by PLK-dependent proteolytic activation of latent TGF-β1 was produced and characterized as reported previously [49].

### Animal experiments

One hundred microliters of saline with or without recombinant VEGF 165 was

injected intravenously via the tail vein of 10-week-old C57BL/6 male mice (n=3) (Japan SLC Inc., Shizuoka, Japan) daily at doses of 10 or 20 μg/kg body weight (BW) for 10 days. Mice were euthanized, and the livers were harvested for biochemical and immunohistochemical analyses. All animal experiments were performed in compliance with protocols approved by the RIKEN Institutional Animal Use and Care Administrative Advisory Committee.

**Staining of liver tissue sections**

Liver tissues were fixed in 4% paraformaldehyde (PFA) and embedded in paraffin, and tissue sections (6-μm thick) were prepared using a Leica sliding microtome (Leica Microsystems, Nussloch, Germany). The liver tissue sections were deparaffinized, rehydrated and incubated for 5 min with a drop of proteinase K (Dako Envision) in 2 ml of 50 mM Tris-HCl buffer (pH 7.5) at RT. Thereafter, endogenous peroxidase was blocked by incubating with 3% hydrogen peroxide in methanol at RT for 10 min. The liver tissue sections were stained with Myer's hematoxylin solution and 1% Eosin Y solution (Muto Pure Chemicals, Tokyo, Japan). For CD31 staining, liver sections were incubated at 4°C overnight with rat anti-CD31 monoclonal antibody (5 μg/ml) and thereafter with biotinylated rabbit anti-rat IgG antibody (1:200) included in the Vectastain Elite ABC kit for 30 min at RT. A 3,3'-diaminobenzidine (DAB) peroxidase substrate kit (Vector Laboratories, Inc., Burlingame, CA, USA) was used

for its chromogenic substrate, which develops as a brown precipitate, to visualize the immunolabeling. For α-SMA staining, liver sections were incubated at 4°C overnight with mouse anti-α-SMA monoclonal antibody (1:100) and thereafter with DAKO Envision's polymer of antibodies labeled with peroxidase for 1 hour at RT. The DAB Peroxidase substrate kit was used for its chromogenic substrate. Sirius red, resulting in a red staining of all fibrillary collagen, was used to evaluate fibrosis. Briefly, the liver sections were stained with 0.05% Fast-green FCF (ChemBlink, Inc., CAS 2353-45-9) and 0.05% Direct red 80 (Polysciences, Inc., CAS 2610-10-18) in saturated picric acid (Muto Pure Chemicals) for 90 min at RT. Positive area analyses were performed using the WinROOF image analysis software from 3 randomly selected fields among 3 mice (total of 9 samples) per group.

**Measurement of hepatic hydroxyproline content**

The hepatic hydroxyproline content was measured as described by Reddy *et al*. [(50)]. Briefly, approximately 40 mg of frozen liver tissue was hydrolyzed in 2 N NaOH for 10 min at 65°C, followed by incubation at 120°C for 20 min. The same amount of 6 N HCl was added and incubated at 120°C for 20 min. Activated charcoal solution (10 mg/ml in 4 N KOH) and 2.2 M acetic acid-0.48 M citric acid buffer (pH 6.5) was added to adjust the pH to 7-8. After centrifugation, 100 mM chloramine T solution was added to the supernatant and incubated at RT for 25 min.

After the addition of 1 M Ehrlich's solution (*p*-dimethylaminobenzaldehyde), samples were incubated at 65 °C for 20 min. Absorbance was measured at 560 nm. The hydroxyproline content was expressed as μg/mg of sample protein.

**Isolation of HSCs and LSECs**

Primary HSCs were isolated from the livers of male C57BL/6 mice by collagenase/pronase digestion and the Nycodenz gradient method, as described previously [(9)]; the cells were then cultured in Dulbecco's modified Eagle's medium (DMEM) containing 10% fetal bovine serum (FBS). Primary LSECs were isolated using a combination of rat anti-CD146 and sheep anti-rat IgG antibodies conjugated with magnetic beads from a fraction separated by a Nicodenz gradient method after collagenase digestion of the livers of male C57BL/6 mice, according to the method described by Kitazume *et al*. [(60)]. The cells were then cultured in DMEM/nutrient mixture F-12 (F12) containing 10% FBS.

**Preparation of LSEC conditioned medium (CM)**

Briefly, $1\times10^5$ LSECs were seeded onto 6-well plates and pre-cultured for 24 hours with DMEM/F12 containing 10% FBS medium to grow the cells to confluency, followed by overnight starvation with DMEM/F12 containing 2% FBS at 37 °C. After the cells were rinsed with phosphate buffered saline (PBS), the medium was

changed to 2 ml of DMEM/F12 containing 2% FBS and further cultured for 24 hours to make LSEC CM.

**Immunofluorescent staining**

HSCs were fixed with 4% PFA for 10 min and incubated with 0.1% Triton X-100 in PBS for 20 min at RT. After blocking with 3% BSA in PBS for 40 min at RT, cells were incubated with FITC-conjugated anti-mouse α-SMA monoclonal antibody (1:200) for 2 hours at RT. After being washed with PBS, cells were mounted with Vectashield DAPI mounting medium (Vector Laboratories, Inc., Burlingame, CA, USA) and observed under the Zeiss LSM 700 laser scanning confocal microscope.

**Determination of the TGF-β concentration in CM**

Measurements of TGF-β were performed using a bioassay (luciferase assay in CCL64 cells) for active TGF-β and an enzyme-linked immunosorbent assay (ELISA) for total TGF-β. CCL64 cells, from the mink lung epithelial cell line, stably expressing $(CAGA)_9$-MLP-luciferase, which contains nine copies of a Smad binding CAGA box element upstream of a minimal adenovirus major late promoter [45], were plated at $2x10^4$ cells/well in a 96-well plate with DMEM containing 10% FBS. On the next day, the medium was replaced with CM harvested from HSCs. After 6 hours, cells were extracted with lysis buffer and luciferase activity was measured using a

Luciferase Assay System (Promega, Madison, WI, USA) according to the manufacturer's instructions. The amount of active TGF-β was calculated from a standard curve made with recombinant TGF-β1. The total TGF-β1 levels present in the LSEC CM before and after incubating with HSCs were determined using a TGF-β1 Emax immune Assay System ELISA kit (Promega, Madison, WI, USA) according to the manufacturer's instructions. Samples were acidified by 1 N HCl to a pH of 3.0 for 15-20 minutes, followed by neutralization with 1 N NaOH before they were subjected to the ELISA.

**Statistics**

Statistical analysis was performed using one-way analysis of variance, followed by the Dunnett's or Tukey's post-hoc test. A two-tailed Student's *t*-test was used to evaluate the differences between the two groups.

# Chapter 4

# Conclusion

Liver fibrosis leads to cirrhosis and eventually to HCC, the most common type of liver cancer in which the five-year relative survival rate is 15%, the second lowest after that in pancreatic cancer [61]. HCV, which is first identified as a cause of non-A and non-B hepatitis in 1989, is a major cause of liver fibrosis associated with an increase in HCC risk. After HCV infection, cirrhosis occurs at a range between 15% and 35% for 25-30 years [62]. Once HCV-induced cirrhosis occurs, HCC develops at an annual rate of 1% to 4%. As another factor promoting liver fibrosis, angiogenesis has been recently focused. However, the precise molecular mechanisms by which either HCV or angiogenesis promote liver fibrosis remain unclear. In this thesis, therefore, the author reported the results of investigation of how these factors promote liver fibrosis.

In chapter 2, the author demonstrated that HCV NS3 protease mimics TGF-β and enhances liver fibrosis via activation of TβRI-Smad signaling pathway. HCV NS3 protease affects the antigenicity and bioactivity of TGF-β2 in $(CAGA)_9$-Luc CCL64 cells, as determined by enhanced luciferase activity, and in human stellate and hepatocyte cell lines, as demonstrated by the up-regulation of TGF-β1 and collagen α1(I) mRNA expression, via binding to TβRI. TNF-α facilitates this mechanism by increasing the colocalization of TβRI with NS3 protease on the surface of HCV-infected cells.

Furthermore, an anti-NS3 antibody against computationally predicted binding sites for TβRI blocked the TGF-β mimetic activities of NS3 in vitro and attenuated liver fibrosis in HCV-infected chimeric mice. These data suggest that HCV NS3 protease mimics TGF-β2 and functions, at least in part, via directly binding to and activating TβRI, thereby enhancing liver fibrosis.

Recently, the direct-acting antiviral agents such as telaprevir and boceprevir, NS3 protease inhibitors, have been used in triple combination therapy with PEGylated interferon and ribavirin. This combination therapy significantly improves sustained virologic response (SVR) rates, defined as continued (24 weeks) undetectable HCV RNA after treatment completion, compared to the treatment with PEGylated interferon and ribavirin alone [(35)]. However, recent studies have reported that the risk of developing HCC remains after SVR, and that high fibrotic stage is an important and independent risk factor for the development of HCC [(63)]. Therefore, the NS3 antibody against the TβRI binding site might have a clinical benefit in HCV patients with cirrhosis after combination therapy.

In chapter 3, the author identified a molecular mechanism by which angiogenesis promotes liver fibrosis. VEGF-treated mice had increased hepatic levels of CD31 and α-SMA expression, hepatic hydroxyproline contents, and R58 LAP-DPs, which is characteristic of cell surface TGF-β activation by PLK. Cultured HSCs expressed

increased levels of α-SMA when incubated with EC conditioned medium but not when incubated directly with VEGF. The increase was partially blocked by the inclusion of neutralizing anti-TGF-β1 antibodies. Either liberating the PLK-uPAR complex from the HSC surface by cleaving a tethering PI-linker with its specific PLC or the inhibition of PLK by camostat mesilate, a serine protease inhibitor, resulted in the inhibition of the activating, latent TGF-β present in LSEC CM and the subsequent HSC activation. These data suggests that angiogenesis may accelerate liver fibrosis at least in part by stimulating the activation of HSCs by providing TGF-β1, which is secreted from increased numbers of ECs and activated on the surface of HSCs by PLK. Furthermore, this study provides new insight into anti-fibrotic therapy by anti-angiogenic agents not limited to sorafenib.

In the end, still one question remains to be answered regarding relationship between HCV and angiogenesis. Recently, Hassan *et al*. reported that HCV core protein mediated the development of hepatic angiogenesis via the production of both TGF-β2 and VEGF by multiple pathways including protein kinase C, E2F1, apoptosis signal-regulating kinase 1, c-jun-N-terminal kinase, extracellular-regulated kinase, and hypoxia inducible factor-1α [(64)]. Therefore, HCV NS3 may also contribute to hepatic angiogenesis via its TGF-β mimetic activity. The author hopes that the anti-NS3

antibody against predicted binding site with TβRI not only addresses this question but also enable to discover further novel biological principles.

**References**


1. Bataller, R., and Brenner, D. A. (2005) Liver fibrosis, *The Journal of Clinical Investigation 115*, 209-218.
2. Friedman, S. L. (2008) Mechanisms of hepatic fibrogenesis, *Gastroenterology 134*, 1655-1669.
3. Friedman, S. L. (2008) Hepatic stellate cells: protean, multifunctional, and enigmatic cells of the liver, *Physiological Reviews 88*, 125-172.
4. Tsukamoto, H. (1999) Cytokine regulation of hepatic stellate cells in liver fibrosis, *Alcoholism, Clinical and Experimental Research 23*, 911-916.
5. Matsuoka, M., Pham, N. T., and Tsukamoto, H. (1989) Differential effects of interleukin-1α, tumor necrosis factor α, and transforming growth factor β1 on cell proliferation and collagen formation by cultured fat-storing cells, *Liver 9*, 71-78.
6. Weiner, F. R., Giambrone, M. A., Czaja, M. J., Shah, A., Annoni, G., Takahashi, S., Eghbali, M., and Zern, M. A. (1990) Ito-cell gene expression and collagen regulation, *Hepatology 11*, 111-117.
7. Breitkopf, K., Lahme, B., Tag, C. G., and Gressner, A. M. (2001) Expression and matrix deposition of latent transforming growth factor β binding proteins in normal and fibrotic rat liver and transdifferentiating hepatic stellate cells in culture, *Hepatology 33*, 387-396.
8. Shi, M., Zhu, J., Wang, R., Chen, X., Mi, L., Walz, T., and Springer, T. A. (2011) Latent TGF-β structure and activation, *Nature 474*, 343-349.
9. Akita, K., Okuno, M., Enya, M., Imai, S., Moriwaki, H., Kawada, N., Suzuki, Y., and Kojima, S. (2002) Impaired liver regeneration in mice by lipopolysaccharide via TNF-α/kallikrein-mediated activation of latent TGF-β,

*Gastroenterology 123*, 352-364.

10. Ikushima, H., and Miyazono, K. (2010) TGFβ signalling: a complex web in cancer progression, *Nature Reviews Cancer 10*, 415-424.
11. Lavanchy, D. (2008) Chronic viral hepatitis as a public health issue in the world, *Best Practice & Research. Clinical Gastroenterology 22*, 991-1008.
12. Moradpour, D., Penin, F., and Rice, C. M. (2007) Replication of hepatitis C virus, *Nature Reviews Microbiology 5*, 453-463.
13. Ploss, A., and Rice, C. M. (2009) Towards a small animal model for hepatitis C, *EMBO reports 10*, 1220-1227.
14. Bartenschlager, R., Lohmann, V., and Penin, F. (2013) The molecular and structural basis of advanced antiviral therapy for hepatitis C virus infection, *Nature Reviews Microbiology 11*, 482-496.
15. Poynard, T., Yuen, M. F., Ratziu, V., and Lai, C. L. (2003) Viral hepatitis C, *Lancet 362*, 2095-2100.
16. Tong, M. J., el-Farra, N. S., Reikes, A. R., and Co, R. L. (1995) Clinical outcomes after transfusion-associated hepatitis C, *The New England Journal of Medicine 332*, 1463-1466.
17. Folkman, J., and Shing, Y. (1992) Angiogenesis, *The Journal of Biological Chemistry 267*, 10931-10934.
18. Ding, B. S., Nolan, D. J., Butler, J. M., James, D., Babazadeh, A. O., Rosenwaks, Z., Mittal, V., Kobayashi, H., Shido, K., Lyden, D., Sato, T. N., Rabbany, S. Y., and Rafii, S. (2010) Inductive angiocrine signals from sinusoidal endothelium are required for liver regeneration, *Nature 468*, 310-315.
19. Thabut, D., and Shah, V. (2010) Intrahepatic angiogenesis and sinusoidal remodeling in chronic liver disease: new targets for the treatment of portal

hypertension?, *Journal of Hepatology 53*, 976-980.

20. Ferrara, N., Gerber, H. P., and LeCouter, J. (2003) The biology of VEGF and its receptors, *Nature Medicine 9*, 669-676.
21. Fernandez, M., Semela, D., Bruix, J., Colle, I., Pinzani, M., and Bosch, J. (2009) Angiogenesis in liver disease, *Journal of Hepatology 50*, 604-620.
22. Medina, J., Arroyo, A. G., Sanchez-Madrid, F., and Moreno-Otero, R. (2004) Angiogenesis in chronic inflammatory liver disease, *Hepatology 39*, 1185-1195.
23. Taura, K., De Minicis, S., Seki, E., Hatano, E., Iwaisako, K., Osterreicher, C. H., Kodama, Y., Miura, K., Ikai, I., Uemoto, S., and Brenner, D. A. (2008) Hepatic stellate cells secrete angiopoietin 1 that induces angiogenesis in liver fibrosis, *Gastroenterology 135*, 1729-1738.
24. Sahin, H., Borkham-Kamphorst, E., Kuppe, C., Zaldivar, M. M., Grouls, C., Al-samman, M., Nellen, A., Schmitz, P., Heinrichs, D., Berres, M. L., Doleschel, D., Scholten, D., Weiskirchen, R., Moeller, M. J., Kiessling, F., Trautwein, C., and Wasmuth, H. E. (2012) Chemokine Cxcl9 attenuates liver fibrosis-associated angiogenesis in mice, *Hepatology 55*, 1610-1619.
25. Yoshiji, H., Kuriyama, S., Yoshii, J., Ikenaka, Y., Noguchi, R., Hicklin, D. J., Wu, Y., Yanase, K., Namisaki, T., Yamazaki, M., Tsujinoue, H., Imazu, H., Masaki, T., and Fukui, H. (2003) Vascular endothelial growth factor and receptor interaction is a prerequisite for murine hepatic fibrogenesis, *Gut 52*, 1347-1354.
26. Chaurushiya, M. S., Lilley, C. E., Aslanian, A., Meisenhelder, J., Scott, D. C., Landry, S., Ticau, S., Boutell, C., Yates, J. R., 3rd, Schulman, B. A., Hunter, T., and Weitzman, M. D. (2012) Viral E3 ubiquitin ligase-mediated degradation of a cellular E3: viral mimicry of a cellular phosphorylation mark targets the

RNF8 FHA domain, *Molecular Cell 46*, 79-90.

27. Marazzi, I., Ho, J. S., Kim, J., Manicassamy, B., Dewell, S., Albrecht, R. A., Seibert, C. W., Schaefer, U., Jeffrey, K. L., Prinjha, R. K., Lee, K., Garcia-Sastre, A., Roeder, R. G., and Tarakhovsky, A. (2012) Suppression of the antiviral response by an influenza histone mimic, *Nature 483*, 428-433.
28. Raney, K. D., Sharma, S. D., Moustafa, I. M., and Cameron, C. E. (2010) Hepatitis C virus non-structural protein 3 (HCV NS3): a multifunctional antiviral target, *The Journal of Biological Chemistry 285*, 22725-22731.
29. Katchalski-Katzir, E., Shariv, I., Eisenstein, M., Friesem, A. A., Aflalo, C., and Vakser, I. A. (1992) Molecular surface recognition: determination of geometric fit between proteins and their ligands by correlation techniques, *Proceedings of the National Academy of Sciences of the United States of America 89*, 2195-2199.
30. Taniguchi, H., Kato, N., Otsuka, M., Goto, T., Yoshida, H., Shiratori, Y., and Omata, M. (2004) Hepatitis C virus core protein upregulates transforming growth factor-β1 transcription, *Journal of Medical Virology 72*, 52-59.
31. Coenen, M., Nischalke, H. D., Kramer, B., Langhans, B., Glassner, A., Schulte, D., Korner, C., Sauerbruch, T., Nattermann, J., and Spengler, U. (2011) Hepatitis C virus core protein induces fibrogenic actions of hepatic stellate cells via toll-like receptor 2, *Laboratory Investigation 91*, 1375-1382.
32. Wu, C. F., Lin, Y. L., and Huang, Y. T. (2013) Hepatitis C virus core protein stimulates fibrogenesis in hepatic stellate cells involving the obese receptor, *Journal of Cellular Biochemistry 114*, 541-550.
33. Presser, L. D., Haskett, A., and Waris, G. (2011) Hepatitis C virus-induced furin and thrombospondin-1 activate TGF-β1: role of TGF-β1 in HCV replication, *Virology 412*, 284-296.

34. Romano, K. P., Laine, J. M., Deveau, L. M., Cao, H., Massi, F., and Schiffer, C. A. (2011) Molecular mechanisms of viral and host cell substrate recognition by hepatitis C virus NS3/4A protease, *Journal of Virology 85*, 6106-6116.

35. Kwong, A. D., Kauffman, R. S., Hurter, P., and Mueller, P. (2011) Discovery and development of telaprevir: an NS3-4A protease inhibitor for treating genotype 1 chronic hepatitis C virus, *Nature Biotechnology 29*, 993-1003.

36. Lecube, A., Hernandez, C., Genesca, J., and Simo, R. (2006) Proinflammatory cytokines, insulin resistance, and insulin secretion in chronic hepatitis C patients: A case-control study, *Diabetes Care 29*, 1096-1101.

37. Toyoda, M., Kakizaki, S., Horiguchi, N., Sato, K., Takayama, H., Takagi, H., Nagamine, T., and Mori, M. (2000) Role of serum soluble Fas/soluble Fas ligand and TNF-α on response to interferon-α therapy in chronic hepatitis C, *Liver 20*, 305-311.

38. Chouteau, P., Defer, N., Florimond, A., Calderaro, J., Higgs, M., Gaudin, A., Merour, E., Dhumeaux, D., Lerat, H., and Pawlotsky, J. M. (2012) Hepatitis C virus (HCV) protein expression enhances hepatic fibrosis in HCV transgenic mice exposed to a fibrogenic agent, *Journal of Hepatology 57*, 499-507.

39. Muller, D. A., and Young, P. R. (2013) The flavivirus NS1 protein: molecular and structural biology, immunology, role in pathogenesis and application as a diagnostic biomarker, *Antiviral Research 98*, 192-208.

40. Zhang, Z. X., Sonnerborg, A., and Sallberg, M. (1994) A cell-binding Arg-Gly-Asp sequence is present in close proximity to the major linear antigenic region of HCV NS3, *Biochemical and Biophysical Research Communications 202*, 1352-1356.

41. Alcon, S., Talarmin, A., Debruyne, M., Falconar, A., Deubel, V., and Flamand, M. (2002) Enzyme-linked immunosorbent assay specific to Dengue virus type

1 nonstructural protein NS1 reveals circulation of the antigen in the blood during the acute phase of disease in patients experiencing primary or secondary infections, *Journal of Clinical Microbiology 40*, 376-381.

42. Xu, L., Hui, A. Y., Albanis, E., Arthur, M. J., O'Byrne, S. M., Blaner, W. S., Mukherjee, P., Friedman, S. L., and Eng, F. J. (2005) Human hepatic stellate cell lines, LX-1 and LX-2: new tools for analysis of hepatic fibrosis, *Gut 54*, 142-151.

43. Zhong, J., Gastaminza, P., Cheng, G., Kapadia, S., Kato, T., Burton, D. R., Wieland, S. F., Uprichard, S. L., Wakita, T., and Chisari, F. V. (2005) Robust hepatitis C virus infection in vitro, *Proceedings of the National Academy of Sciences of the United States of America 102*, 9294-9299.

44. Kuo, T. F., Tatsukawa, H., Matsuura, T., Nagatsuma, K., Hirose, S., and Kojima, S. (2012) Free fatty acids induce transglutaminase 2-dependent apoptosis in hepatocytes via ER stress-stimulated PERK pathways, *Journal of Cellular Physiology 227*, 1130-1137.

45. Datta, P. K., and Moses, H. L. (2000) STRAP and Smad7 synergize in the inhibition of transforming growth factor β signaling, *Molecular and Cellular Biology 20*, 3157-3167.

46. Tatsukawa, H., Fukaya, Y., Frampton, G., Martinez-Fuentes, A., Suzuki, K., Kuo, T. F., Nagatsuma, K., Shimokado, K., Okuno, M., Wu, J., Iismaa, S., Matsuura, T., Tsukamoto, H., Zern, M. A., Graham, R. M., and Kojima, S. (2009) Role of transglutaminase 2 in liver injury via cross-linking and silencing of transcription factor Sp1, *Gastroenterology 136*, 1783-1795 e1710.

47. Soderberg, O., Leuchowius, K. J., Gullberg, M., Jarvius, M., Weibrecht, I., Larsson, L. G., and Landegren, U. (2008) Characterizing proteins and their interactions in cells and tissues using the in situ proximity ligation assay,

*Methods 45*, 227-232.

48. Tateno, C., Yoshizane, Y., Saito, N., Kataoka, M., Utoh, R., Yamasaki, C., Tachibana, A., Soeno, Y., Asahina, K., Hino, H., Asahara, T., Yokoi, T., Furukawa, T., and Yoshizato, K. (2004) Near completely humanized liver in mice shows human-type metabolic responses to drugs, *The American Journal of Pathology 165*, 901-912.
49. Kojima, S. (2008) Detection of hepatic fibrogenesis targeting proteolytic TGF-β activation reaction, *Hepatology*, p 917A.
50. Reddy, G. K., and Enwemeka, C. S. (1996) A simplified method for the analysis of hydroxyproline in biological tissues, *Clinical Biochemistry 29*, 225-229.
51. Mejias, M., Garcia-Pras, E., Tiani, C., Miquel, R., Bosch, J., and Fernandez, M. (2009) Beneficial effects of sorafenib on splanchnic, intrahepatic, and portocollateral circulations in portal hypertensive and cirrhotic rats, *Hepatology 49*, 1245-1256.
52. Mandriota, S. J., Seghezzi, G., Vassalli, J. D., Ferrara, N., Wasi, S., Mazzieri, R., Mignatti, P., and Pepper, M. S. (1995) Vascular endothelial growth factor increases urokinase receptor expression in vascular endothelial cells, *The Journal of Biological Chemistry 270*, 9709-9716.
53. Breuss, J. M., and Uhrin, P. (2012) VEGF-initiated angiogenesis and the uPA/uPAR system, *Cell Adhesion & Migration 6*, 535-615.
54. Colman, R. W. (2006) Regulation of angiogenesis by the kallikrein-kinin system, *Current Pharmaceutical Design 12*, 2599-2607.
55. Lee, J. S., Semela, D., Iredale, J., and Shah, V. H. (2007) Sinusoidal remodeling and angiogenesis: a new function for the liver-specific pericyte?, *Hepatology 45*, 817-825.

56. Neef, M., Ledermann, M., Saegesser, H., Schneider, V., Widmer, N., Decosterd, L. A., Rochat, B., and Reichen, J. (2006) Oral imatinib treatment reduces early fibrogenesis but does not prevent progression in the long term, *Journal of Hepatology 44*, 167-175.

57. Thabut, D., Routray, C., Lomberk, G., Shergill, U., Glaser, K., Huebert, R., Patel, L., Masyuk, T., Blechacz, B., Vercnocke, A., Ritman, E., Ehman, R., Urrutia, R., and Shah, V. (2011) Complementary vascular and matrix regulatory pathways underlie the beneficial mechanism of action of sorafenib in liver fibrosis, *Hepatology 54*, 573-585.

58. Wood, J. M., Bold, G., Buchdunger, E., Cozens, R., Ferrari, S., Frei, J., Hofmann, F., Mestan, J., Mett, H., O'Reilly, T., Persohn, E., Rosel, J., Schnell, C., Stover, D., Theuer, A., Towbin, H., Wenger, F., Woods-Cook, K., Menrad, A., Siemeister, G., Schirner, M., Thierauch, K. H., Schneider, M. R., Drevs, J., Martiny-Baron, G., and Totzke, F. (2000) PTK787/ZK 222584, a novel and potent inhibitor of vascular endothelial growth factor receptor tyrosine kinases, impairs vascular endothelial growth factor-induced responses and tumor growth after oral administration, *Cancer Research 60*, 2178-2189.

59. Ferrara, N., Hillan, K. J., Gerber, H. P., and Novotny, W. (2004) Discovery and development of bevacizumab, an anti-VEGF antibody for treating cancer, *Nature Reviews Drug Discovery 3*, 391-400.

60. Kitazume, S., Imamaki, R., Ogawa, K., Komi, Y., Futakawa, S., Kojima, S., Hashimoto, Y., Marth, J. D., Paulson, J. C., and Taniguchi, N. (2010) α2,6-sialic acid on platelet endothelial cell adhesion molecule (PECAM) regulates its homophilic interactions and downstream antiapoptotic signaling, *The Journal of Biological Chemistry 285*, 6515-6521.

61. Siegel, R., Naishadham, D., and Jemal, A. (2013) Cancer statistics, 2013, *CA:*

*a cancer journal for clinicians 63*, 11-30.

62. El-Serag, H. B., and Rudolph, K. L. (2007) Hepatocellular carcinoma: epidemiology and molecular carcinogenesis, *Gastroenterology 132*, 2557-2576.

63. Chang, K. C., Hung, C. H., Lu, S. N., Wang, J. H., Lee, C. M., Chen, C. H., Yen, M. F., Lin, S. C., Yen, Y. H., Tsai, M. C., Tseng, P. L., and Hu, T. H. (2012) A novel predictive score for hepatocellular carcinoma development in patients with chronic hepatitis C after sustained response to pegylated interferon and ribavirin combination therapy, *The Journal of Antimicrobial Chemotherapy 67*, 2766-2772.

64. Hassan, M., Selimovic, D., Ghozlan, H., and Abdel-kader, O. (2009) Hepatitis C virus core protein triggers hepatic angiogenesis by a mechanism including multiple pathways, *Hepatology 49*, 1469-1482.

**Acknowledgements**

本論文は、著者が慶應義塾大学大学院理工学研究科後期博士課程在学中に行った研究成果をまとめたものです。本研究を行うにあたり、多大なる御指導、御鞭撻を賜りました慶應義塾大学理工学部教授　井本正哉博士に謹んで感謝の意を表します。

本研究を遂行するにあたり、終始御懇切な御指導、御鞭撻を賜りました理化学研究所ライフサイエンス技術基盤研究センター特別ユニットリーダー小嶋聡一博士に謹んで感謝の意を表します。

本論文の執筆にあたり、御指導、御助言を頂きました慶應義塾大学理工学部教授　岡浩太郎博士、慶應義塾大学理工学部准教授　土居信英博士、慶應義塾大学理工学部准教授　清水史郎博士に心より厚く御礼申し上げます。

また、本研究に際し多くの御助言を頂きました慶應義塾大学専任講師田代悦博士に深く感謝いたします。

HCV ならびに HCV 易感染肝癌細胞株をご供与くださり、またウイルス学的見地から御指導、御助言をいただきました国立感染症研究所ウイルス第二部脇田隆字博士、相崎英樹博士に深く感謝いたします。

組換え NS3 タンパク質をご供与いただきました理化学研究所　横山茂之博士、白水美香子博士、松本武久博士、寺田貴帆博士、津曲千恵美氏に深謝いたします。

NS3 と TGF-β 受容体の結合解析に際し、多大なる御指導、御協力を賜りました山梨大学医学部教授　宮澤恵二博士、矢口壮一氏に厚く御礼申し上げます。また同結合について、ドッキングシミュレーションによる解析を行なっていただきました同研究所　髙谷大輔博士に深く感謝いたします。

抗 NS3 抗体の作製ならびに同抗体を用いた動物実験に際し、多大なる御指導、御支援を賜りました理化学研究所　山口時男博士に厚く御礼申し上げます。

また、臨床的見地から多大なる御指導、御助言いただきました東京慈恵会医科大学教授　松浦知和博士、浜松医科大学教授　鈴木哲朗博士に深く感謝いたします。

初代培養細胞の単離、培養に際し、多大なる御指導、御助言をいただきました理化学研究所　原詳子氏、李殷瑞博士に深く御礼申し上げます。三年間を通じてお二方に日々濃密な議論を重ねていただけたことに感謝いたします。また、血管新生による肝線維化促進機構の解析に際し、多大なるご助力をいただきました同研究所　江田諭氏（現：㈱ファンケル）に深謝いたします。

日々の研究生活を様々な面でサポートしていただきました理化学研究所アシスタント　田島貴美枝さん、高山康代さん、多くのことを学ばせていただいた理化学研究所　辰川英樹博士（現：名古屋大学)、古谷裕博士、秦咸陽博士、そして後輩、スタッフの皆様に感謝いたします。

ケミカルバイオロジー研究室の一員として私を温かく受入れていただき、また刺激をいただいた同研究室卒業生　笹澤有紀子博士、新荘聡子博士をはじめとする諸先輩方、同期の藤巻貴宏君、後輩の皆様、そして秘書の梅崎秀香さんに感謝いたします。

社会人博士課程への進学に際し、多大なる御支援、御助力を賜りました湧永製薬株式会社代表取締役社長　湧永寛仁氏、同社取締役副社長　湧永寛信氏、同社特別研究顧問　岡孝巳博士をはじめ社員の皆様に厚く御礼申し上げます。

最後に、研究生活を常に支えてくれた最愛なる妻と娘、そして両親に心より感謝いたします。